People's Democratic Republic of Algeria
Ministry of Higher Education and Scientific Research

University M'Hamed BOUGARA – Boumerdes

Institute of Electrical and Electronic Engineering

Department of Power and Control

Final Year Project Report Presented in Partial Fulfilment of
the Requirements for the Degree of the

MASTER

In **Control Engineering**

Option: **Control Engineering**

Title:

Parameters Identification of Bifacial PV Cells Under Different Irradiations

Presented by:

- **LAGAB Sarra Oumnia**

Supervisor:

Pr. KHELDOUN Aissa

Co-Supervisor:

Dr. BELMADANI Hamza

Registration Number: 2022/2023

Abstract

Given the non-linear characteristics of photovoltaic modules (PV) and their dependency on operating conditions, it becomes crucial to accurately forecast their behavior under varying temperatures and irradiance. As the demand for this technology continues to grow, it is imperative to develop effective methods for precisely extracting the intrinsic parameters of these modules. To help in design and assess the performance of PV panels, a developed model is used. The model is none other than an equivalent electrical circuit with basic components (a source, resistors, and one diode or more). Single-diode and double-diode models are the most popular in the literature. In this project, these models are used to model the bifacial photovoltaic cell. Equivalent circuit parameters must be obtained, from either a set of experimental data or a manufacturer's data sheet, in order to construct a model. The aim is to obtain values that yield an accurate model. The problem is tackled as an optimization one, where the sum of Root mean square error (RMSE), between the experimental and the calculated data, and the power error around the maximum power point (MPP) is the function to be optimized. Optimization is achieved using two different meta-heuristic algorithms: Marine Predators Algorithm (MPA) and Snake Optimizer Algorithm(SOA). The aforementioned algorithms are adapted to extract the bifacial PV parameters $(a_f, I_{0f}, I_{phf}, R_{pf}, R_{sf}, a_r, I_{0r}, I_{phr}, R_{pr}, R_{sr})$ using MATLAB.

Dedication

I dedicate this work to the person who believed in me the most and taught me the importance of hard work my mother.
To my father who did his best so I can be here .
To my siblings Ibtihel and Abdeldjallil for their continuous support.
To the memories of my grandparents whom I would never forget.
To my dearest friends Sife and Ines whose unwavering support and encouragement have been instrumental in my journey.

Acknowledgements

This project was realized at the Institute of Electrical and Electronics Engineering at the University of Boumerdes and was accomplished under the supervision of Pr. KHELDOUNE.A

I would like to express my deep gratitude and warm thanks to my supervisor who have guided and oriented me throughout the achievement of this work.

Furthermore, I extend my thanks to Dr. Belmadani.H who has done his best to transmit his knowledge and help.

Contents

List of Figures

List of Tables

List of Abbreviations

AC Alternating Current.

AM Air Mass.

BSC Bifcial Solar Cell.

BSF Back Surface Field.

DC Direct Current.

DDM Double Diode Model.

DE Differentiel Evolution.

EVA Ethylene-Vinyl Acetate.

FF Fill Factor.

FTO Fluorine-doped Tin Oxide.

HIT Heterojunction with Intrinsic Thin laye.

IBC Interdigitated Back Contact.

ITO Indium Tin Oxide.

KCL Kirchhoff's Current Law.

MPA Marine Predators Algorithm.

MPP Maximum Power Point.

PERC Passivated Emitter and Rear Contact.

PERL Passivated Emitter and Rear Locally Diffused.

PERT Passivated Emitter and Rear Totally Diffused.

PSO Particle Swarm Optimization.

PV Photovoltaic.

RMSE Root Mean Square Error.

SDM Single Diode Model.

SOA Snake Optimizer Algorithm.

STC Standard Test Conditions.

TCO Transparent Conductive Oxide.

Nomenclature

η	Efficiency
a	Diode ideality factor
a_f	Front ideality factor
a_r	Rear ideality factor
G	Irradiation
I_0	Diode saturation current
I_D	Diode current
I_{0f}	Front saturation current
I_{0r}	Rear saturation current
I_{mpp}	Current at maximum power
I_{phf}	Front photocurrent
I_{phr}	Rear photocurrent
I_{ph}	Photo-generated current
I_{sc}	Short-circuit current
k	Boltzmann's constant 1.38064852×10^{-23}
P_{in}	Input power
P_{max}	Maximum power
q	Elementary charge $1.6\times10^{-19}C$
R_p	PV model Shunt resistance
R_s	PV model Series resistance
R_{pf}	Front shunt resistance
R_{pr}	Rear shunt resistance
R_{sf}	Front series resistance
R_{sr}	Rear series resistance
T	Temperature
V_{mpp}	Voltage at maximum power
V_{oc}	Open-circuit voltage

General Introduction

The world is experiencing rapid development, accompanied by an ever-increasing demand for power[1]. However, meeting this demand often comes at the cost of increased pollution. Fortunately, there is a growing interest in environmentally friendly alternatives for electricity generation. Among these alternatives, photovoltaics (PV) have gained significant attention due to their ability to convert solar energy into electricity. As the cost of PV panels decreases and their efficiency improves, more individuals and companies are investing in this renewable energy source.
Solar power offers a dependable and consistent energy source due to the permanent and stable presence of the sun. This renewable energy solution has gained recognition as a clean and nonpolluting alternative in response to the urgent global warming issue. Furthermore, the long operational lifespan of solar photovoltaic (PV) installations, lasting up to 30 years or more with minimal maintenance[2], significantly reduces operating costs and renders them insignificant when compared to conventional power technologies. The essence of solar power lies in the conversion of light into electricity through the utilization of semiconducting materials that exhibit the photovoltaic effect. This conversion occurs at the fundamental level of a PV system, namely the PV cell, which serves as the basic building block for harnessing solar energy.
In this study, the focuse is on the bifacial solar modules which absorb sunlight from both sides (front and back). Bifacial solar cells can reduce the cell cost in a photovoltaic system since their utilization rate is higher, it is expected that the use of bifacial solar cell modules will become wider since they have better performance and better cost. Bifacial panels outperform traditional one-faced panels throughout the year,under ideal conditions, bifacial panels can produce (32%) more energy [3].
The performance of photovoltaic systems relies heavily on the specific operating conditions under which they are deployed. Variations in temperature and irradiance, influenced by seasonal and geographical factors, can lead to fluctuations in the electrical output.
In response, researchers have dedicated efforts to developing appropriate models for simulating and predicting the behavior of photovoltaic (PV) cells and modules under various circumstances. These models play a crucial role in the design, manufacturing, and evaluation of PV systems. One essential aspect for ensuring the reliability of these models lies in accurately estimating their parameters. In this project, our focus is on extracting the parameters of the single diode model for bifacial modules under different irradiation levels. Obtaining precise parameter values is vital for achieving reliable predictions and assessments, ultimately enhancing the overall performance and efficiency of PV systems. Through this work the Marine Predators Algorithm and the Snake Optimizer Algorithm will be used.
The project is structured as follows:

Chapter One provides a comprehensive background on the principles and construction of photovoltaic systems. It also highlights the significance of PV panel parameters and addresses the challenges associated with this technology.

Chapter two focuses on the bifacial cells, their structure, and working principle along with an explanation of the mathematical and electrical model using the diode model. It also mentions both advantages and problems facing this technology.

Chapter three explores the objective function to be minimized,gives a detailed description for the optimization algorithms employed to extract the intrinsic ten

parameters of the single-diode model for bifacial cells.

Chapter four shows the result of applying the two used algorithm at identifying the ten single diode model parameters at each of the different irradiation levels, along with a discussion of the obtained results and a brief comparison between the two algorithms.

The report culminates with a general conclusion including proposals for future work.

Chapter One: Photovoltaic System Principles

1.1 Introduction

Solar energy is regarded as a prominent and abundant source of renewable energy, holding great potential for facilitating a more environmentally sustainable future. Its benefits include being a freely available energy resource that can be harnessed through photovoltaic panels, contributing to the reduction of air pollution. However, it is essential to acknowledge the existing disadvantages associated with solar energy, which will be discussed in the latter part of this chapter.

The first chapter of this research provides a comprehensive overview of solar energy, delving into its fundamental principles and exploring the operation of photovoltaic cells. Furthermore, the chapter presents an analysis of the characteristics and parameters of solar cells, along with an examination of the conventional models employed in the study of photovoltaic panels.

1.2 Photovoltaic Term

The term "Photovoltaic" originates from the combination of the words "photo," meaning light, and "voltaic," referring to voltage. It is a technology that directly converts solar energy into electricity and is commonly abbreviated as PV. This process involves the use of semiconductor devices, also known as solar cells, which convert sunlight into direct current (DC) electricity. PV cells are typically arranged in modules or arrays, and they have various applications, ranging from charging batteries and powering small electronics like calculators to providing electricity to homes. Additionally, PV systems can generate alternating current (AC) if equipped with inverters, which convert DC power to AC power.

1.3 Photovoltaic Cells

1.3.1 Structure

The fundamental composition of a photovoltaic (PV) cell comprises multiple layers of semiconductor material, predominantly silicon, which is widely employed in PV cell fabrication.

The uppermost layer of the cell consists of a thin anti-reflective coating, facilitating enhanced absorption of sunlight. Beneath lies a layer of p-type silicon, a semiconductor material characterized by positively charged "holes" representing electron deficiencies. Adjacent to the p-type layer lies the depletion region or p-n junction, which serves as a thin region of separation between the p-type and n-type layers.

The n-type layer, comprising another semiconductor material, houses freely movable, negatively charged electrons. The interface between the p-type and n-type layers is where the photovoltaic effect takes place, enabling the conversion of light energy into electrical energy.

Metal contacts positioned at the top and bottom of the PV cell enable the extraction of the generated electrical energy. When sunlight impinges upon the cell, electrons are dislodged from the atoms within the material, thereby instigating an electric current that can be harnessed to power electronic devices or stored in batteries.

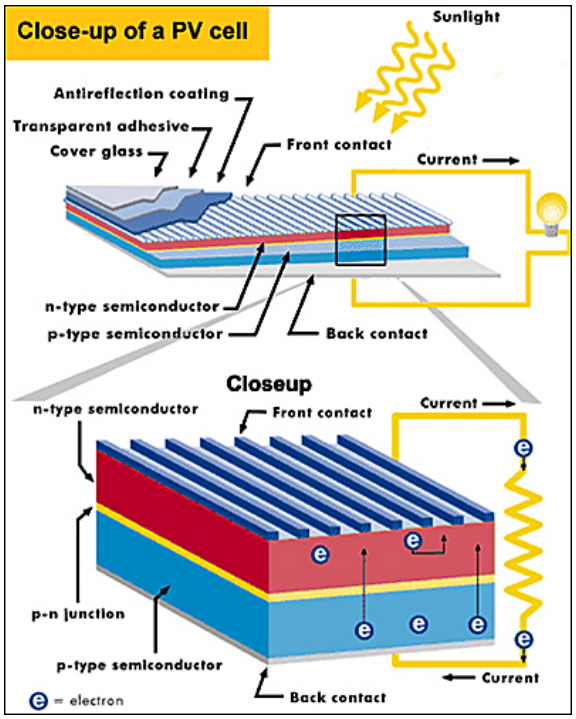

Figure 1.1: Structure of a photovoltaic

1.3.2 Technologies

PV technology has continuously advanced and will continue to do so in the future, leading to the emergence of many types of PV cells[4].

- Monocrystalline silicon cells
  Monocrystalline silicon cells, which are made of pure silicon crystal with a continuous lattice and almost no defects, have been around the longest and offer high efficiency in light conversion (up to 22-24%). However, they are expensive due to the complicated manufacturing process, and they are also brittle[5].

- Polycrystalline cells
  are made of multiple grains and plates of silicon crystals and have lower efficiency (12%) but are less expensive to manufacture[5].

- Amorphous silicon cells
  are produced by depositing silicon film onto substrate glass, resulting in less silicon usage and lower conversion efficiency (6%)[5].

- Acadmium telluride cells
  have become popular due to their lower cost per kW-hour, but they have a limited supply of tellurium and potentially toxic impact of cadmium at the stage of disposal. Copper indium gallium selenide cells do not contain toxic cadmium and have higher efficiency (just under 20%), but mass production has been challenging.[4]

- polymer and organic PV cells
  are lightweight and flexible, but less efficient (about 1/3 of a typical Si cell efficiency) and have shorter service life.[4]

While these are the main types of PV technology, research and innovation will lead to the emergence of new and better types of PV cells in the future. The breakthroughs in the PV industry are dependent on developments in other fields such as chemistry.

1.3.3 PV Effect

A solar cell is essentially a semiconductor diode that spans a large area. This diode is created by adding impurities, or "doping," into the semiconductor crystal to form a P-N junction. The P-region is doped with boron atoms, while the N-region is doped with phosphorus atoms. This doping process creates an excess of free electrons in the N-region and a surplus of free holes in the P-region.

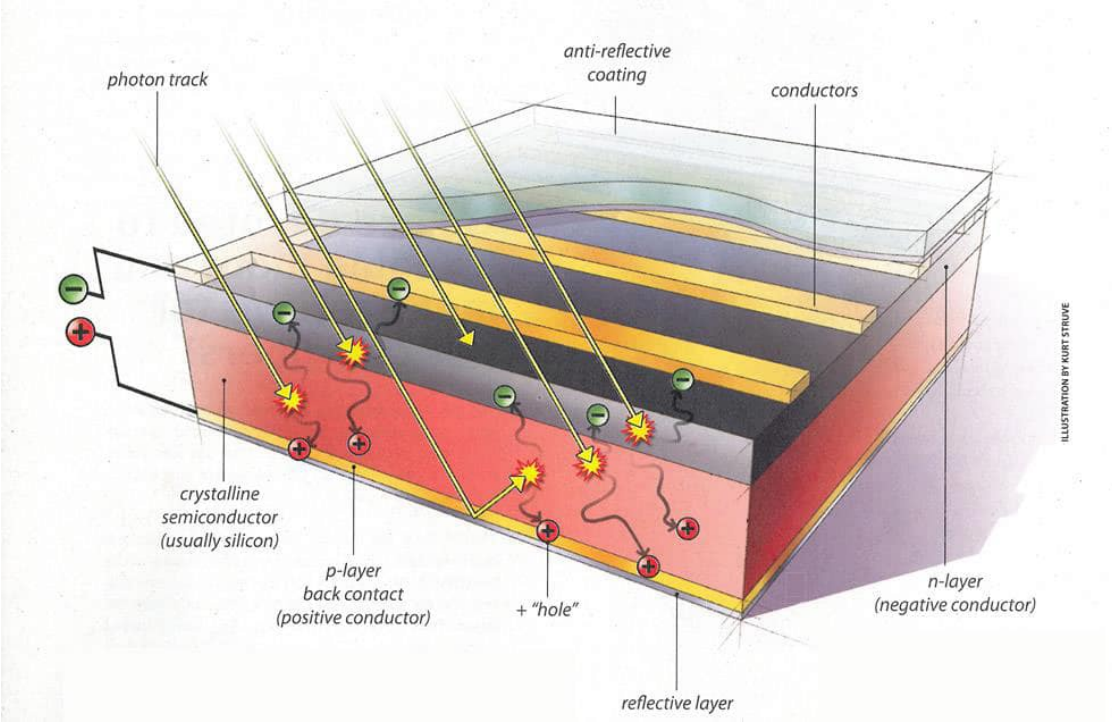

Figure 1.2: Photovoltaic effect diagram

When photons strike the PN junction, they generate pairs of opposite electrical charge carriers (electrons and holes). These carriers are separated due to the presence of the PN junction and move in opposite directions, with electrons moving toward the N-region and holes moving toward the P-region. This creates a voltage across the junction, which leads to the formation of a stable electric cell that can produce a current and power output[6].

The current and power output of a solar cell depends on its efficiency, size, and the intensity of sunlight striking its surface. Under open-circuit, no-load conditions, a typical silicon PV cell produces about 0.5-0.6 v DC, which may not be sufficient to charge batteries or run motors. Due to this, they are available in the form of modules or panels to provide sufficient voltage and current for real life applications; as shown in the next section[6][7].

1.3.4 Types of PV devices

Since a single PV cell can only generate a limited amount of electricity, and so to increase the electricity collected to a point where it is enough to use in everyday applications, a number of cells can be interconnected in a sealed, weatherproof package called a panel/module. So, when multiple solar cells are connected as an integrated group, all oriented in one plane, a solar photovoltaic panel or module is created. In general, it can be said that the number of series cells indicates the voltage of the module, whereas the number of parallel cells indicates the current. To further increase the collected voltage and current, PV modules can be wired in series and parallel into what is called a PV array[8].

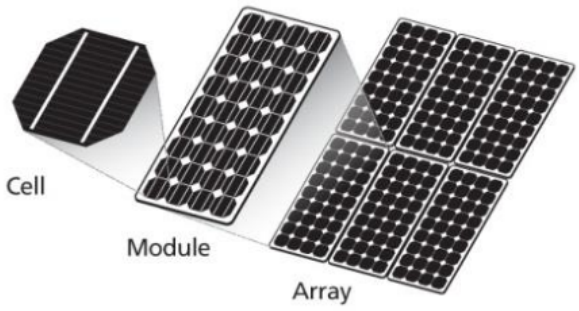

Figure 1.3: Cell,Module,Array[8]

1.3.5 The Electrical Characteristics of the PV Cell

PV module manufacturers provide the electrical properties of their products based on specific conditions called standard test conditions (STC). These conditions are established with a cell temperature of 25°C, irradiation level of 1000 W/m2, and air mass value represented by AM = 1.5, which measures the impact of air mass on the spectral distribution and intensity of sunlight. Under these conditions, the current versus voltage relationship of a PV panel working uniformly can be illustrated using the following curves :

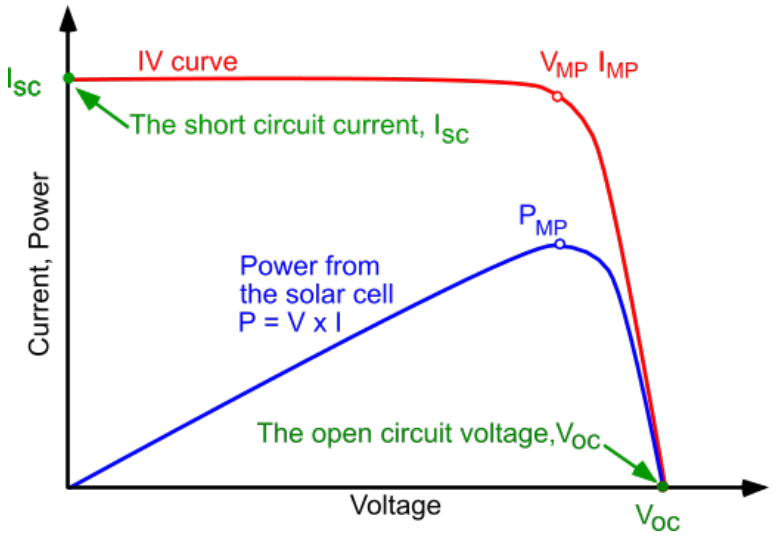

Figure 1.4: I-V and P-V curve of a photovoltaic cell

i. I-V P-V Curves

The I-V curve of a PV module displays the potential combinations of current and voltage outputs. The power generated in a DC electrical circuit is the product of current and voltage :

$$P\,(\text{Watts}) = I\,(\text{Amperes}) \times V\,(\text{Volts}) \tag{1.1}$$

When there is no resistance in the circuit, a solar panel produces its maximum current, known as the Short Circuit Current (Isc).
Conversely, the Open Circuit Voltage (Voc) is obtained when there is infinite resistance, resulting in zero current. The Isc and Voc occur at opposite ends of the load resistance range and are represented on the I-V curve, with current on the vertical axis and voltage on the horizontal axis.

The power output can be calculated at any point on the I-V curve, with zero output at both the Isc and Voc points. The Maximum Power Point (MPP) occurs at the knee of the I-V curve, where maximum power output is obtained, designated by Vmpp and Impp.

To model a PV cell, the three important points are: the maximum current at zero voltage, the maximum voltage without a charge, and the maximum power output.

ii. Fill Factor

The maximum current and voltage that a photovoltaic cell can generate are the short-circuit current and open-circuit voltage, respectively. However, at these points, the power output of the solar cell is zero. To express the maximum power produced by a solar cell in terms of Voc and Isc, a parameter known as the fill factor (FF) is used. FF is defined as the ratio of the maximum power from the solar cell to the product of Voc and Isc[9].

The fill factor is directly affected by the values of the cell's series, shunt resistances and diodes losses. Increasing the parallel resistance (Rp) and decreasing the series resistance (Rs) lead to a higher fill factor, thus resulting in greater efficiency, and bringing the cell's output power closer to its theoretical maximum. The reason for which the fill factor is calculated by comparing the maximum power to the theoretical power (PT) that would be output at both the open circuit voltage and short circuit current together.

$$FF = \frac{I_{mpp}V_{mpp}}{I_{sc}V_{oc}} \tag{1.2}$$

iii. Efficiency

Solar cell efficiency is a commonly used parameter to compare the performance of different solar cells. Efficiency is defined as the ratio of the output power, Pout, from the solar cell to the solar power input, Pin, into the PV cell. Since the PV cell can operate up to its maximum power, Pout can be taken as Pmax. Pin is determined as the product of the irradiance of the incident light with the surface area of the solar cell [9]. The efficiency not only reflects the performance of the solar

cell but also depends on the spectrum and intensity of the incident sunlight and the temperature of the solar cell. Therefore, the conditions under which efficiency is measured must be carefully controlled to compare the performance of one device to another. This is typically done under STC conditions. The efficiency is calculated using the following equation:

$$\eta = \frac{V_{oc} I_{sc} FF}{P_{in}} \tag{1.3}$$

1.4 PV models

1.4.1 Ideal Model

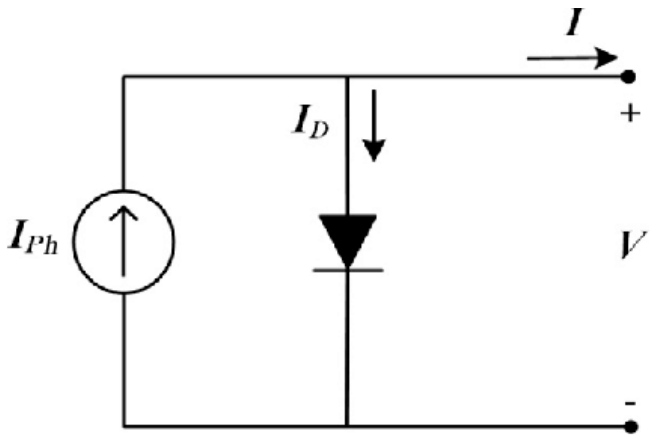

Figure 1.5: Ideal solar cell model

With the presence of irradiation, the p–n junction absorbs the photon from incident light and generates electron–hole pairs (or carriers) as previously explained in the photovoltaic effect section. the resulting electrical current known as the photocurrent, Iph. The inclusion of Iph into the Shockley equation forms an elementary description of an illuminated cell that comprises of a current source connected in parallel to a p–n junction diode. This is known as the ideal model, as shown in Fig1.5. The output current of the cell is given by

$$I = I_{\text{ph}} - I_D \tag{1.4}$$

Where I_D is the diode current. :

$$I_D = I_0 \left[\exp\left(\frac{V}{aV_t} \right) - 1 \right] \tag{1.5}$$

where I_0 is the reverse diode saturation current and V is the PV model outputted voltage. Moreover, n denotes the ideality factor of the diode and V_t is thermal voltage which is obtained as follows :

$$V_t = \frac{kT}{q} \tag{1.6}$$

$$I = I_{\text{ph}} - I_0 \left[\exp\left(\frac{V}{aV_t} \right) - 1 \right] \tag{1.7}$$

1.4.2 Single Diode Model

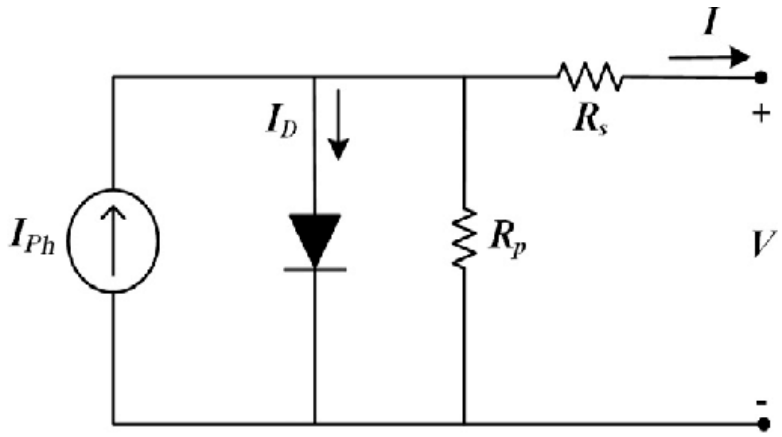

Figure 1.6: One diode solar cell model

While the solar cell can be considered as ideal in theory, in reality, it deviates from the ideal characteristics. To provide more accurate analysis, better models have been developed. Equation (1.7) is not capable of accurately describing the behavior of a PV cell. The single-diode model shown in Figure 1.6 is a more practical and improved model that incorporates series and parallel resistances in the previous model. While this model takes more computational time, it produces more precise results. The output current is given by eq (1.8).
By applying KCL :

$$I = I_{\text{ph}} - I_D - I_p \tag{1.8}$$

$$I = I_{\text{ph}} - I_0 \left[\exp\left(\frac{V + IR_s}{aV_t}\right) - 1\right] - \frac{V + IR_s}{R_p} \tag{1.9}$$

1.4.3 Double Diode Model

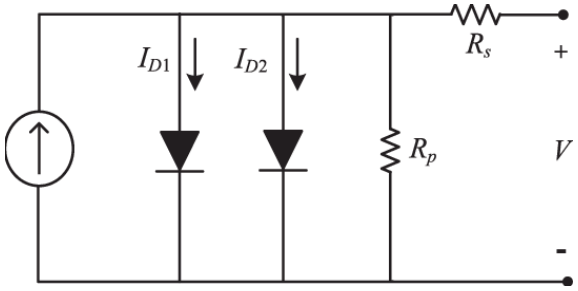

Figure 1.7: Two diode solar cell model

This model is a modified version of the previous one by adding a second diode in parallel with the first one as shown in Fig 1.7. The additional diode stands for the effect caused by the recombination that takes place in the space-charge zone by introducing another diode in parallel. However, the two-diode model makes computations longer despite its accuracy. Eq (1.11) in this case gives the output current:

$$I = I_{\text{ph}} - I_{D1} - I_{D\check{s}} - I_p \tag{1.10}$$

$$I = I_{ph} - I_{01}\left[\exp\left(\frac{V + IR_s}{a_1V_t}\right) - 1\right] - I_{02}\left[\exp\left(\frac{V + IR_s}{a_2V_t}\right) - 1\right] - \frac{V + IR_s}{R_p} \tag{1.11}$$

1.5 PV Model Parameters

1.5.1 Photo-Current I_{ph}

Photo-current pertains to the electric current that ensues as a consequence of light absorption within the semiconductor material.

The amplitude of the photo-current relies on various factors, including the intensity and wavelength of the incident light, the characteristics of the material itself, and the existence of external influences like applied voltage or temperature.

1.5.2 Diode Saturation Current I_0

The saturation current is a combination of the generation current caused by thermal generation of electron-hole pairs within the depletion region of the diode and the diffusion current due to minority carriers in the n and p regions diffusing across the depletion region. Although the saturation current is voltage independent, it does depend on temperature since both the current contributions depend on thermally stimulated carriers[10].

1.5.3 Ideality Factor a

The ideality factor (a) is a unitless parameter. It is a measure of how closely the diode follows the ideal diode equation. It accounts for the different mechanisms responsible for moving carriers across the junction. The value of n equal to one means the transport process is purely diffusion, and a value equal to two if it is primarily recombination in the depletion region. The parameter n represents one of parameters to be computed in our work. The ideality factor appears in the diode current component of equation.

1.5.4 Series Resistance Rs

The presence of series resistance in a solar cell can be attributed to three primary factors. Firstly, it arises from the flow of current through the emitter and base regions of the solar cell. Secondly, it arises from the contact resistance between the metal contact and the silicon material. Lastly, it arises from the resistance encountered at the top and rear metal contacts. The primary consequence of series resistance is the reduction of the fill factor, although excessively high values can also lead to a decrease in the short-circuit current.

It is important to note that series resistance does not impact the solar cell at open-circuit voltage, as the overall current flow through the cell, including the series resistance, is negligible. However, as the operating voltage approaches the open-circuit voltage, the I-V curve of the solar cell is significantly influenced by the presence of series resistance. A straightforward approach to estimating the series resistance of a solar cell involves determining the slope of the IV curve at the open-circuit voltage point[11].

1.5.5 Shunt Resistance Rsh

The occurrence of power losses in solar cells due to the presence of a shunt resistance (Rp) is commonly attributed to manufacturing defects rather than deficiencies in

solar cell design. The shunt resistance provides an alternative pathway for the light-generated current, resulting in a decrease in the current flowing through the solar cell junction and a reduction in the solar cell voltage. The impact of the shunt resistance is particularly noticeable under low light conditions, where there is a diminished light-generated current, leading to a higher loss of current to the shunt. Furthermore, the effect of a parallel resistance becomes more prominent at lower voltages when the effective resistance of the solar cell is elevated.

1.6 Effect of Temperature

Solar energy encompasses both light and heat components, and although the amount of solar energy reaching a PV panel remains unaffected by temperature, its conversion into electrical energy is influenced. With rising temperature, the band gap energy diminishes, consequently impacting the semiconductor parameters. This reduction in the band gap prompts an elevation in the energy of electrons, facilitating easier bond dissociation with a reduced energy requirement to transition from a lower to a higher energy state. Among the parameters of a solar cell, the open circuit voltage is primarily impacted by temperature increases. The impact of temperature on the I-V curve is illustrated in the figure presented below[12].

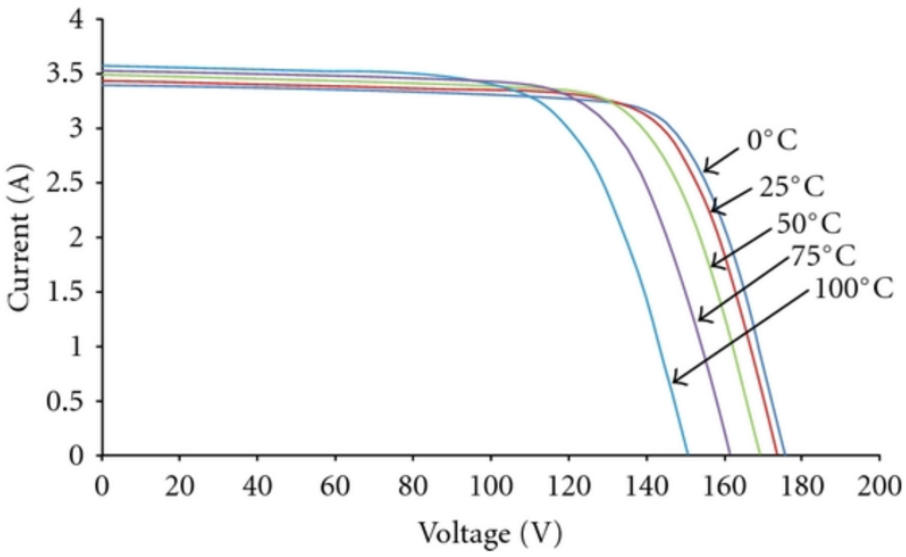

Figure 1.8: I-V curves depending on temperature[12]

1.7 Effect of Light Intensity

The PV cell parameters are highly sensitive to changes in light intensity. Even a slight variation in light intensity can affect the short circuit current, the open circuit voltage, the fill factor, the efficiency, and the impact of both the series and shunt resistances. The standard test light intensity is 1 kW/m^2 or AM 1.5. Daily variations in light intensity are common and can have significant impacts on solar cells. At low light levels, the shunt resistance plays a more important role. As light intensity decreases, the current in the PV cell also decreases, causing its equivalent resistance

to approach the value of the shunt resistance. When these two resistances become equal, the amount of current flowing through the shunt resistance increases, leading to an increase in the fractional power loss caused by the shunt resistance. Therefore, on a cloudy day, a solar cell with a high shunt resistance retains a greater fraction of its original power than a solar cell with a low shunt resistance.

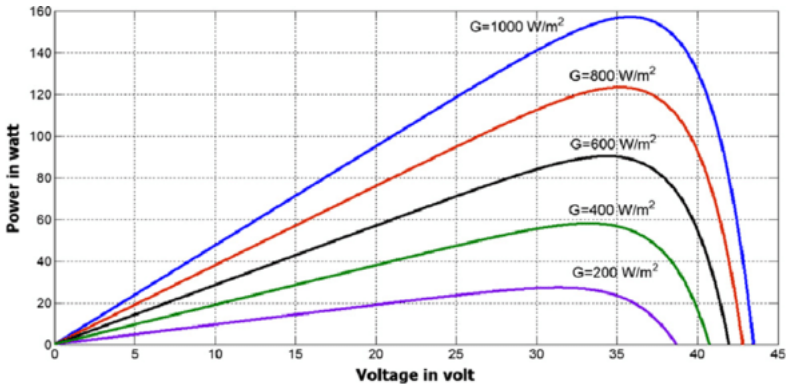

Figure 1.9: P-V curves depending on irradiation

1.8 Conclusion

Solar energy, a renewable source, possesses the ability to convert sunlight into electricity through the utilization of photovoltaic panels. While this conversion process may exhibit certain drawbacks in specific scenarios, solar energy boasts a multitude of advantages over conventional energy sources such as oil and coal. Consequently, it is widely regarded as the foremost energy source for the future sustainability of our planet.

This chapter has provided an overview of the theoretical process involved in the conversion of solar energy and has explored the various parameters of photovoltaic panels and their impact on power output. Additionally, the concept of efficiency has been discussed, highlighting its dependence on external conditions such as temperature and light intensity, as well as on specific parameters.

To model the photovoltaic cell and determine its parameters, equivalent circuits have been employed. Several of these circuits have been introduced in this chapter, including the single diode model and the double diode model. Mathematical relationships describing the current-voltage characteristics have been derived from these circuits. However, solving these equations presents challenges due to their inherent nonlinearity. For this reason,researchers have endeavored to develop the global algorithms aimed at identifying the required parameters.

Chapter Two : Bifacial Solar Cells

2.1 Introduction

The increasing demand for renewable energy sources has led to the development of new and innovative solar technologies. One such technology is bifacial solar cells which differ from traditional monofacial solar cells in that they can generate electricity from both the front and back sides of the cell. This allows them to harness sunlight reflected from the surrounding environment.

this chapter will provide a comprehensive overview of the design and materials used in bifacial solar cells, as well as the principles underlying their operation. By investigating the model parameters of bifacial solar cells, a deeper understanding of their performance characteristics and the factors that influence their efficiency will be provided. Furthermore, this chapter will explore the various structures and configurations employed in bifacial solar cells, highlighting their potential for enhanced energy generation through the utilization of both incident and reflected light.

2.2 Bifacial Solar Cells

Bifacial solar cells are made of crystalline silicon, just like traditional solar cells. However, unlike traditional solar cells, bifacial solar cells have a transparent conductive oxide (TCO) layer on the backside of the cell, which allows light to pass through and be absorbed by the silicon[13]. This means that bifacial solar cells can generate electricity not only from the direct sunlight that hits the front side of the cell but also from the diffuse and reflected sunlight that hits the backside of the cell.

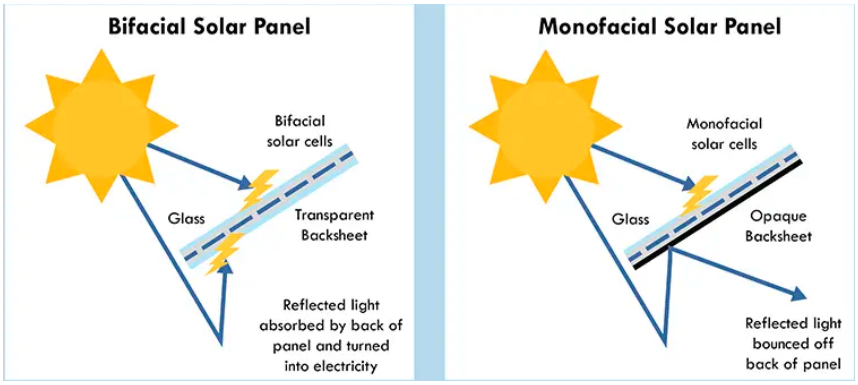

Figure 2.1: Bifacial solar cells

2.3 Bifacial Cells Structure

Bifacial solar cells have a similar basic structure to traditional solar cells, with some additional features to enable light absorption from both the front and back sides. The typical structure of a bifacial solar cell includes:

- **Front Contact**
  The front contact of the bifacial solar cell is usually a transparent conductive oxide (TCO) layer, such as indium tin oxide (ITO) or fluorine-doped tin oxide (FTO). This layer allows sunlight to pass through while providing an electrical connection and collecting the current generated in the front side of the cell[14].

- **Front-Side Semiconductor**
  The front side of the bifacial solar cell consists of a semiconductor material, typically crystalline silicon (c-Si), which is widely used in solar cell technology. The front side is doped to create a p-n junction, which facilitates the separation and flow of photogenerated carriers (electrons and holes) when exposed to sunlight[15].

- **Front-Side Passivation Layer**
  To reduce surface recombination and improve the efficiency of the front side, a passivation layer is often applied. This layer, commonly made of silicon nitride (SiNx) or silicon oxide (SiOx), helps to minimize the loss of charge carriers at the surface of the front-side semiconductor[14].

- **Back-Side Semiconductor**
  The back side of the bifacial solar cell also consists of a semiconductor material, typically lightly doped to enable better light transmission. The back-side semiconductor can be the same material as the front side or a different material optimized for back-side absorption, such as amorphous silicon (a-Si) or microcrystalline silicon (c-Si)[15].

- **Back Contact**
  The back contact of the bifacial solar cell is usually a conductive layer that allows for electrical collection of the current generated on the back side. It is often made of a metal grid or a thin metal film, such as aluminum (Al) or silver (Ag), to provide good electrical conductivity[14].

- **Encapsulation**
  Bifacial solar cells are typically encapsulated to protect them from environmental factors such as moisture, dust, and mechanical stresses. Encapsulation layers can consist of a front and back encapsulant, usually made of a transparent polymer material such as ethylene-vinyl acetate (EVA) or encapsulant sheets, to provide mechanical strength and ensure long-term durability.

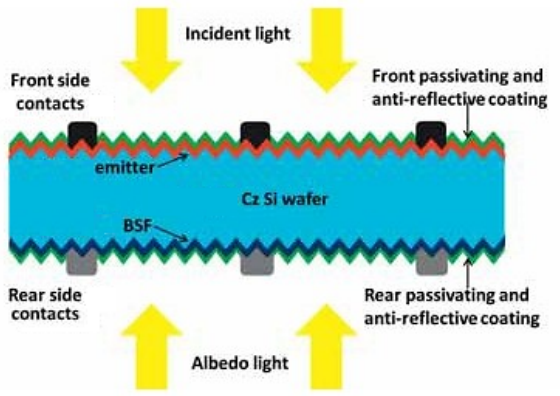

Figure 2.2: Bifacial solar cell structure

It's important to note that the specific structure and materials used in bifacial solar cells can vary depending on the manufacturing process and the desired performance characteristics. Different technologies, such as monocrystalline, polycrystalline, or thin-film, can be adapted to bifacial configurations to achieve optimal energy generation from both sides of the cell

2.4 Bifacial Cells Working Principle

Bifacial solar cells work on the principle of capturing sunlight not only from the front side but also from the back side of the cell, increasing the overall energy generation. The key working principle of bifacial solar cells can be summarized as follows:

- **Front-Side Absorption**
  Like traditional solar cells, the front side of a bifacial solar cell is designed to absorb sunlight. It consists of a semiconductor material, such as silicon, with a p-n junction that generates an electric current when illuminated by photons. Sunlight incident on the front side is partially reflected, absorbed, or transmitted through the cell.

- **Back-Side Absorption**
  Bifacial solar cells have an additional feature that allows them to capture sunlight from the back side as well. The back side of the cell is usually designed with a transparent or lightly doped material that allows light to pass through. When sunlight reaches the back side, it can be reflected or transmitted through the front side, or it can interact with the active material on the back side, leading to additional current generation.

- **Enhanced Light Capture**
  Bifacial solar cells can benefit from enhanced light capture due to various mechanisms. The back side can receive sunlight reflected from surrounding surfaces, such as the ground or nearby structures, increasing the overall energy yield. Moreover, diffused light that enters the cell from all directions can reach the back side, enabling energy generation even under non-optimal sun angles or cloudy conditions.

- **Electrical Connection**
  The front and back sides of the bifacial solar cell are electrically connected in parallel or series to ensure proper current flow and maximize the overall energy output. The electrical contacts collect the current generated by both sides and deliver it to the external load or power conversion system.

- **System Design Considerations**
  To optimize the performance of bifacial solar cells, several factors must be considered during system design. These include the angle of incidence of sunlight, cell orientation and tilt, ground albedo (reflectivity), and shading effects. By carefully considering these factors, the energy yield of bifacial solar cells can be maximized.

Overall, the principle behind bifacial solar cells revolves around capturing sunlight from both the front and back sides of the cell, thereby increasing the total energy generation compared to traditional solar cells. This feature makes bifacial solar cells well-suited for certain applications, such as ground-mounted installations or building-integrated photovoltaics, where they can take advantage of reflected and diffused light to boost overall efficiency[16].

2.5 Bifacial Solar Cell Types

- **Passivated Emitter and Rear Contact (PERC)**
  The PERC cell configuration involves the deposition of a layer of Al2O3 on the backside of the wafer, followed by the deposition of SiN over the Aluminum Oxide layer to establish a passivation layer. Subsequently, laser-induced holes are created in this passivation layer to generate localized Back Surface Field (BSF). Finally, a metal contact is applied on the backside of the wafer, resembling the process used in standard poly-Si cells[17].

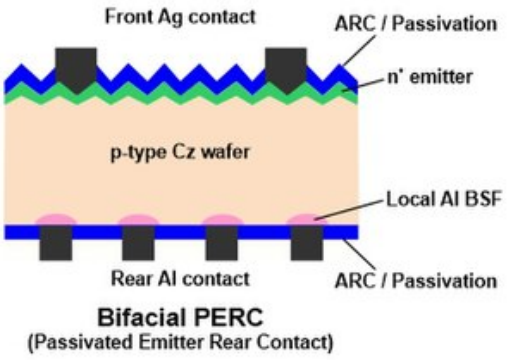

Figure 2.3: Bifacial PERC

- **Passivated Emitter and Rear Totally Diffused (PERT)**
  PERT cells employ a co-diffusion technique that simultaneously forms the emitter and the back surface field, effectively mitigating the emergence of critical shunts at the device edges[18].

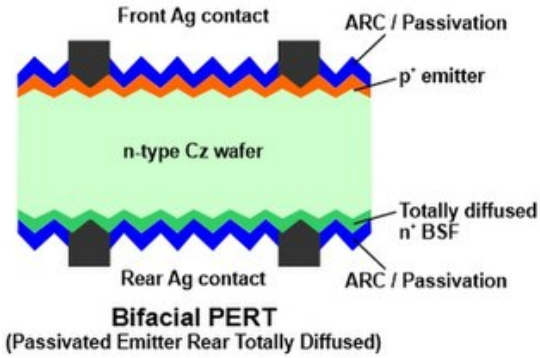

Figure 2.4: Bifacial PERT

- **Passivated Emitter and Rear Locally Diffused (PERL)**
  PERL cells are developed based on the PassDop methodology, wherein the rear surface undergoes localized diffusion with phosphorus to establish a back surface field (BSF)[18].

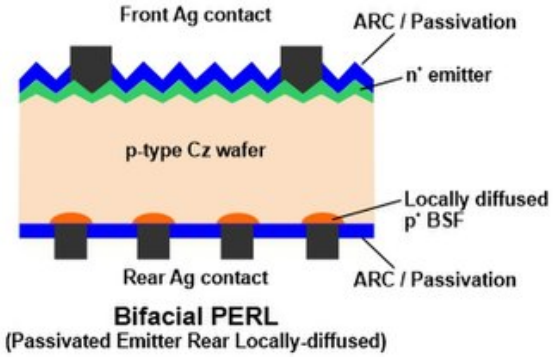

Figure 2.5: Bifacial PERL

- **Heterojunction with Intrinsic Thin layer (HIT)**
  HIT cells incorporate a thin intrinsic layer sandwiched between a p-type and an n-type layer, resulting in reduced recombination losses[19].

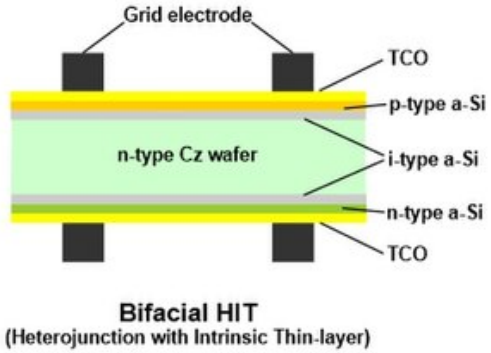

Figure 2.6: Bifacial HIT

- **Interdigitated Back Contact (IBC)**
  IBC cells feature both front and back contacts positioned on the backside of the cell, effectively minimizing shading losses and enhancing overall efficiency[20].

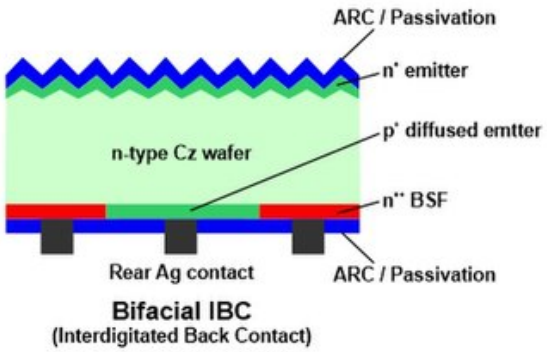

Figure 2.7: Bifacial IBC

The table below shows the efficiency of each technology [21] along with their bifaciality factor or coefficient which represents a measure of the ability of a solar cell to generate electricity from both sides. It is calculated by dividing the power generated by the rear side of the cell by the power generated by the front side of the cell. The higher the bifaciality coefficient, the more efficient the solar cell is at generating electricity from both sides[22].

Bifacial solar cell technology	Front-side efficiency	Rear-side efficiency	Bifaciality factor
PERC	21.2 - 22.7%	15.4-18.6%	69-82%
PERL	19.8%	17.6%	89%
PERT	18.6 - 23.2%	15.3-18.6%	80-87.5%
IBC	20.9 - 22%	15.6-18.3%	74-83%
HIT	23%	22%	95%

Table 2.1: Bifacial Solar Cell Technologies[20]

2.6 Modelling Bifacial Solar Cells

Modelling bifacial solar cells involves developing mathematical models and simulation techniques that accurately represent the physical and electrical behavior of these cells. These models take into account various factors such as cell structure, materials, optical properties, and electrical parameters. By simulating the operation of bifacial solar cells under different environmental conditions, modelling provides valuable insights into their performance, efficiency, and energy yield. As seen previously on the first chapter,the diode model parameters can fully describe the behaviour of photovoltaic cells.In this section,the electrical model mentionned previously will be applied on the bifacial solar cells (to simplify the equation and simulation the single diode model was chosen)[23].

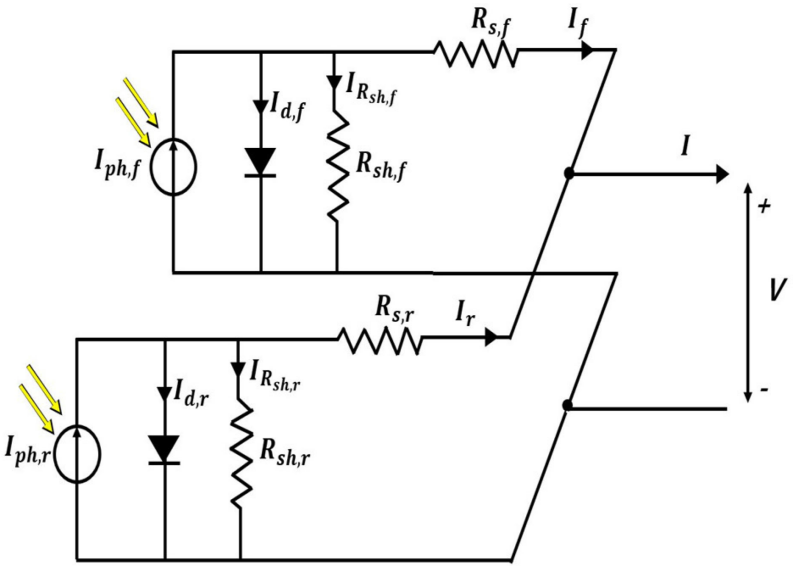

Figure 2.8: Equivalent circuit for a bifacial solar cell[23].

To establish a model for bifacial module, two single diode models were considered each for front and rear side IV characterization of the module. Two single diode models are mounted in parallel to represent the bifacial technology and the influence of each side on the other. By applying KCL on both sides the same way as Eq (1.8) :

$$I_f = I_{\text{phf}} - I_{Df} - I_{pf} \tag{2.1}$$

$$I_r = I_{\text{phr}} - I_{Dr} - I_{pr} \tag{2.2}$$

Similarly the equation is the same as Eq.9 for the front and rear currents. The total current of a bifacial solar cell can be represented by the sum of the current (I_f) generated by the absorbed light from the front, and the current (I_r) generated by the absorbed light from the rear [23], as shown in Fig 2.8 with the following equation:

$$I_{cell} = I_f + I_r \tag{2.3}$$

$$\begin{aligned} I = I_{phf} - I_{0f}\left[\exp\left(\frac{V + IR_{sf}}{n_f V_t}\right) - 1\right] - \frac{V + IR_{sf}}{R_{pf}} + \\ I_{phr} - I_{0r}\left[\exp\left(\frac{V + IR_{sr}}{n_r V_t}\right) - 1\right] - \frac{V + IR_{sr}}{R_{pr}} \end{aligned} \tag{2.4}$$

The parallel connection of the front and rear single diode models signifies the simultaneous operation of both sides in generating electricity. It acknowledges that the rear side can receive reflected and diffuse light from the surroundings, thereby contributing to the overall energy generation of the module. The influence of each side on the other is taken into account, allowing for a more comprehensive analysis and accurate prediction of the module's performance.

2.7 Irradiation Effect on Bifacial Solar Cell

The effect of irradiation on bifacial solar modules differs from that on traditional ones. They have the unique capability of capturing light from both the front and back sides,as mentionned previously, allowing them to generate electricity from both direct sunlight and reflected or diffuse light.
Here are some of the key impacts :

Increased Energy Generation: Higher light intensity, especially when combined with highly reflective surfaces (e.g., snow, white ground), can significantly enhance the energy generation of bifacial modules. The additional light captured from the rear side can contribute to increased power output.

Rear Side Contribution: Bifacial modules can generate a considerable portion of their power from the rear side illumination, which is reflected or scattered light. As light intensity increases, more light is available for capture on the rear side, further contributing to the overall power output.

Albedo Effect: Albedo refers to the reflectivity of the ground or surrounding surfaces. Bifacial modules benefit from high albedo conditions, such as snow-covered ground or light-colored surfaces, as they reflect more light onto the rear side of the module. This can result in a significant boost in energy generation.

Angle of Incidence: The angle at which light strikes the module, known as the angle of incidence, can affect the performance of bifacial modules. Higher light intensity often corresponds to a lower angle of incidence, which can increase the amount of light captured by the rear side of the module and consequently enhance its power output.

Shading Considerations: While higher light intensity generally benefits bifacial modules, it is essential to consider potential shading issues. Shadows from nearby objects or structures can obstruct the light from reaching the rear side of the module, reducing its energy generation. Careful system design and installation practices are necessary to minimize shading and maximize the performance of bifacial modules.

In summary, increased light intensity can lead to higher energy generation in bifacial solar modules due to their ability to capture light from both the front and back sides. Factors such as albedo, angle of incidence, and shading need to be considered to optimize the performance of bifacial modules under different light intensity conditions.

2.8 Advantages of BSC

Bifacial solar panels offer several advantages over conventional monofacial solar arrays. It should be noted that to maximize their performance, installation near highly reflective surfaces such as swimming pool glass, sandy, stone, or snowy areas is recommended.

One of the key advantages of bifacial solar panels is their superior performance[24]. By generating electricity from both sides of the panel, they exhibit a significant increase in overall energy generation compared to conventional solar panels. When mounted on a highly reflective surface, the additional power produced from the rear side can lead to a claimed increase in output of up to 30%.

Durability is another notable advantage of bifacial panels. Unlike traditional monofacial panels, bifacial panels are frameless and feature tempered glass covering on both sides. This design makes them more resilient and able to withstand harsh weather conditions, high temperatures, strong winds, and UV exposure. The tempered glass provides weather and UV resistance, enhancing their long-term durability.

Bifacial panels also perform well in diffuse light conditions, further setting them apart from monofacial panels. The increased surface area allows them to capture and convert more light, making them economically advantageous in terms of long-term costs.

Additionally, bifacial solar panels often come with longer warranty periods, typically up to 30 years. This extended warranty coverage provides added peace of mind and ensures the longevity of the investment.

In summary, bifacial solar panels offer improved performance, durability, efficiency in diffused light, and extended warranty periods compared to conventional monofacial panels. These advantages make them an attractive option for harnessing solar energy and enhancing overall system performance.

2.9 Disadvantages of BSC

While bifacial solar panels offer numerous advantages, they also come with some potential disadvantages that should be considered. These include:

Complex installation requirements: To maximize the benefits of bifacial panels, they need to be installed in specific locations with highly reflective surfaces. This requirement adds complexity to the installation process and may limit the deployment options in certain settings.

Variable performance dependence: The performance of bifacial panels is highly dependent on environmental factors such as the angle of incidence, shading, and the quality of the reflective surface. In suboptimal conditions, such as when the panels are installed in areas with low reflectivity or high shading, the energy output from the rear side may not be significant enough to justify the added cost.

Limited compatibility with existing systems: Bifacial panels may not be compatible with certain existing mounting systems or infrastructure, requiring modifications or additional investments to integrate them effectively.

Maintenance challenges: Bifacial panels, with their double-sided glass construction, may require more regular cleaning and maintenance compared to monofacial panels. This is especially true for the rear side, which is exposed to dirt, dust, and potential accumulation of debris.

It is important to evaluate these disadvantages alongside the benefits when considering the adoption of bifacial solar panels. The decision should be based on the specific project requirements, site conditions, and cost-effectiveness considerations.

2.10 Conclusion

In conclusion, bifacial solar technology presents a promising solution for maximizing energy generation and increasing the efficiency of photovoltaic systems. The understanding of the structure, working principle, and modeling approaches discussed in this chapter contributes to the knowledge base surrounding bifacial solar cells. By further exploring the advantages, addressing the disadvantages, and advancing modeling techniques, researchers and industry professionals can unlock the full potential of bifacial solar technology, driving the transition towards a sustainable and clean energy future.

Chapter three : Parameters Identification Using Metaheuristic Algorithms

3.1 Introduction

As seen in both chapters One and two, in order to model a PV module/cell several parameters must be deduced. Modeling holds significance, be it for educational objectives or for accurately evaluating the performance of a PV panel.Parameters extraction of photovoltaic models, which remains a multi-variable, nonlinear, and multi-modal problem especially since the studied case is bifacial solar cells, can be accomplished using global search algorithms. The algorithms explained in this chapter are :
- MPA which is a new metaheuristic algorithm developed in 2019 and published in 2020, even used for forecasting confirmed cases of COVID-19 in Italy, USA, Iran and Korea[25].
- SOA which is is a metaheuristic algorithm proposed by [26] in 2022 to mimic the mating behavior of snakes. They have been adapted to suite the purpose of bifacial solar cell parameters identification of single diode model using experimental data.

3.2 Objective Function Formulation

The electrical parameters of the SDM model of PV module can be identified using the optimization approach, which essentially needs a definition of the objective function. The proper structure of the objective function is essential for precise identification of unknown parameters. The extracted parameters should guarantee that the model exactly simulates the PV cell/panel.In this study, the objective function proposed to optimally design the ten parameters of such model is the Root Mean Square Error (RMSE) between experimental and estimated currents. RMSE is given by the equation :

$$RMSE(\theta) = \sqrt{\frac{1}{N}\sum_{i=1}^{N}(I_{i,measured} - I_{i,estimated})^2} \tag{3.1}$$

N: is the number of points measured (I_i, V_i).
$I_{i,measured}$: is the measured current.
$I_{i,estimated}$: is the estimated current.
θ=$[a_f, I_{0f}, I_{phf}, R_{pf}, R_{sf}, a_r, I_{0r}, I_{phr}, R_{pr}, R_{sr}]$: parameters to estimate.

RMSE is the the most used objective functions in PV parameters extraction [27] ,as the objective function may cause some imperfections around the MPP ,in order to avoid this problem the error at the MPP between the maximum power measured and the maximum power estimated was introduced. The objective function becomes :

$$F(\theta) = RMSE + \alpha * (P_{max,measured} - P_{max,estimated})^2 \tag{3.2}$$

α : the weight multiplied to the power error to have an effect on the objective function.
F(θ): is the objective function to minimize.

3.3 Global Search Algorithms : Metaheuristics

There are many options for classifying optimization algorithms. Mainly, they can be classified into two categories, which are: Local optimization algorithms and Global optimization algorithms. In our work ,the algorithm used is a global optimazation one. The process of globally optimizing a function or a set of functions is guided by specific criteria. Typically, a set of boundaries and constraints are considered to optimize the decision variables. This approach differs from regular optimization methods as it aims to identify the maximum or minimum across all possible input values, rather than local extrema [28]. Unlike other optimization techniques that focus on local optima, global optimization algorithms do not require an initial guess and yield more accurate results by efficiently discovering and utilizing the global optima of the cost function.

In this project, metaheuristics are employed. Metaheuristics are adaptable methods that can effectively tackle a wide range of optimization problems. These techniques are designed to find high-quality solutions from a vast space of feasible solutions, offering computational efficiency compared to other optimization methods. In the next section the used technique will be fully discussed.

3.4 Marine Predator Algorithm

The Marine Predator Algorithm (MPA) is a nature-inspired optimization method that imitates the hunting strategies of marine predators like sharks and dolphins. Its goal is to solve optimization problems by leveraging the techniques used by these predators to search for and capture prey.

3.4.1 MPA Mechanisms

MPA relies on the principle of survival of the fittest, where predators must choose the best strategy to outperform prey confrontation rates. In MPA, predators actively search for prey while the prey itself seeks its food[29]. Many animals employ a stochastic foraging strategy, where the next location is determined by the current position and the transition probability to the next position. This optimal strategy has evolved in marine ecosystems and has been adopted by predators for survival. Marine creatures such as sharks, swordfish, and tunas exhibit Lévy-like behavior when searching for prey, which is an effective strategy for locating patchy prey in nature. Predators use a Lévy approach in areas with lower prey density and switch to Brownian movement in environments with abundant prey.
The MPA is a population-based approach. The initial randomization of the MPA is similar to different metaheuristics algorithms, in which the candidate's position is updated as follows:

$$X_0 = X_{min} + rand(X_{max} - X_{min}) \tag{3.3}$$

where X_{max} and X_{min} are the upper and lower limit of design variable,respectively,and $rand$ represents a random vector that its upper and lower bounds $\in [0, 1]$
According to the survival of the fittest strategy, top predators are highly gifted in the foraging process. Therefore, the optimal solution is specified as a top predator to arrange Elite. Such Elite supervises in seeking and finding the prey related to

the knowledge of prey's locations.

$$Elite = [X^I_{1,1} X^I_{1,2} X^I_{1,d}; .....; X^I_{n,1} X^I_{n,2} X^I_{n,d}] \tag{3.4}$$

where $\overrightarrow{X^I}$ is a vector consisting of the highest-performing predators, which reproduce n times to form the Elite group. The variables n and d represent the number of agents and dimensions, respectively. The Elite is updated during each iteration if a better predator replaces the current top predator.

The Prey is structured in a way that aligns with the dimensions of the Elite. Predators update their positions based on the Prey. To initialize the process, the fittest predator organizes the Elite, and this arrangement establishes the initial Prey. The Prey can be described as follows:

$$Prey = [X_{1,1} X_{1,2} X_{1,d}; .....; X_{n,1} X_{n,2} X_{n,d}] \tag{3.5}$$

where X_{ij} is the j-th dimension of the i-th prey .The optimization process heavily relies on both the Elite and the Prey. The Marine Predator Algorithm (MPA) utilizes random variables and operators to facilitate exploration and prevent being trapped in local minima.

3.4.2 MPA Optimization Stages

The MPA optimization process incorporates three distinct phases that emulate the life cycle of predators and prey in nature. The transition between these phases is determined by the velocity ratio between prey and predator. The first stage is characterized by a high-velocity ratio, while the second and third stages exhibit unity and low-velocity ratios, respectively. Each phase is associated with a specific number of iterations, aligning with the movement patterns observed in nature. Let's delve into each of these stages:

- **Stage 1 : High-Velocity Ratio**
  In the initial iterations of the optimization process, the prey exhibits a higher velocity compared to the predator (a high-velocity ratio). This phase is focused on exploration, emphasizing the need to explore the search space extensively. In this high-velocity phase (v $\geq$ 10), the predator remains stationary while the prey moves rapidly in search of optimal solutions. The mathematical model representing this phase is illustrated as follows [29][30]:

  For Iter $<\frac{1}{3}$ Iter$_{max}$

  $$\overrightarrow{stepsize_i} = \overrightarrow{R_B} \otimes (\overrightarrow{Elite_i} - \overrightarrow{R_B} \otimes \overrightarrow{Prey_i}) \tag{3.6}$$

  where i= 1,2....n

  $$\overrightarrow{Prey_i} = \overrightarrow{Prey_i} + P.\overrightarrow{R} \otimes \overrightarrow{Stepsize_i} \tag{3.7}$$

  The velocity ratio between prey and predator is represented by v. The vector $\overrightarrow{R_B}$ represents the Brownian movement, depicting a normal distribution. The symbol $\otimes$ indicates element-wise multiplication. P is a constant value of 0.5, and represents a vector of random numbers ranging from 0 to 1. Iter and IterMax denote the current iteration and the maximum number of iterations, respectively. This scenario occurs during one-third of the optimization process iterations, characterized by a high step-size or movement speed to enhance exploration capabilities[31].

- **Stage 2 : Unity-Velocity Ratio**
  During this stage, the predator and prey move at an equal velocity, replicating the behavior of both searching for their respective food sources. This phase occurs in the middle of the optimization process. In this scenario, half of the population is dedicated to exploration, while the other half focuses on exploitation. The prey primarily handles exploitation, while the predator takes charge of exploration. For v $\approx$ 1, the prey moves according to Lévy distributions, whereas the predator follows Brownian motion. Mathematically, this phase is described as follows [30]:

  For $\frac{1}{3}Iter_{max}<Iter<\frac{2}{3}Iter_{max}$
  For the first half of the population;

$$\overrightarrow{stepsize_i} = \overrightarrow{R_L} \otimes (\overrightarrow{Elite_i} - \overrightarrow{R_L} \otimes \overrightarrow{Prey_i}) \tag{3.8}$$

  where i= 1,2....n/2

$$\overrightarrow{Prey_i} = \overrightarrow{Prey_i} + P.\overrightarrow{R} \otimes \overrightarrow{stepsize_i} \tag{3.9}$$

  The vector $\overrightarrow{R_L}$ represents a set of random numbers associated with Lévy movement. The term $\overrightarrow{R_L} \otimes \overrightarrow{Prey_i}$ imitates the prey's movement using the Lévy approach, where the inclusion of the prey's location step size simulates its motion.

  For the second half of the population :

$$\overrightarrow{stepsize_i} = \overrightarrow{R_B} \otimes (\overrightarrow{R_B} \otimes \overrightarrow{Prey_i} - \overrightarrow{Prey_i}) \tag{3.10}$$

  where i=n/2,....n

$$\overrightarrow{Prey_i} = \overrightarrow{Elite_i} + P.CF \otimes \overrightarrow{stepsize_i} \tag{3.11}$$

  where CF is the parameter that controls the step size of movement for the predator.
  The term $\overrightarrow{R_B} \otimes \overrightarrow{Prey_i}$ emulates the predator's movement using the Brownian approach, allowing the prey to update its location based on the predator's motion characterized by Brownian motion[30].

- **Stage 3 : Low-Velocity Ratio**
  During this phase, the predator moves faster than the prey. It represents the final scenario in the optimization process and is associated with intensive exploitation. In the case of a low-velocity ratio (v=0.1), the predator's movement follows a Lévy distribution. This phase is mathematically described as follows [30]-[32]:

  For $Iter > \frac{2}{3}Iter_{max}$

$$\overrightarrow{stepsize_i} = \overrightarrow{R_L} \otimes (\overrightarrow{R_L} \otimes \overrightarrow{Elite_i} - \overrightarrow{Prey_i}) \tag{3.12}$$

  where i=1,....n

$$\overrightarrow{Prey_i} = \overrightarrow{Elite_i} + P.CF \otimes \overrightarrow{stepsize_i} \tag{3.13}$$

By utilizing the Lévy approach, the term $\overrightarrow{R_L} \otimes \overrightarrow{Elite_i}$ emulates the predator's movement.By incorporating the step size into the Elite's location, the prey's position is updated to simulate the predator's motion.

3.4.3 Eddy Formation and FADs' Effect

Environmental factors, such as the formation of eddies or the influence of Fish Aggregating Devices (FADs), can induce behavioral changes in marine predators. The effect of FADs is mathematically expressed as:

$$\overrightarrow{Prey_i} = \begin{cases} \overrightarrow{Prey_i} + CF[\overrightarrow{X_{min}} + \overrightarrow{R} \otimes (\overrightarrow{X_{max}} - \overrightarrow{X_{min}})] \otimes \overrightarrow{U}, & \text{if } r < FADs, \\ \overrightarrow{Prey_i} + [FADs(1-r) + r](\overrightarrow{Prey_{r1}} - \overrightarrow{Prey_{r2}}), & \text{if } r > FADs. \end{cases} \tag{3.14}$$

Here, FADs = 0.2 represents the probability of FADs' effect on the optimization process. U is a binary vector containing elements of zero and one. It is generated by creating a random vector within the range [0,1] and setting the elements to zero if they are less than 0.2, and one if they are greater than 0.2. r is a random number from a uniform distribution within the range [0,1]. $\overrightarrow{X_{min}}$ and $\overrightarrow{X_{max}}$ are vectors that define the lower and upper bounds of the dimensions. The subscripts r1 and r2 represent random indexes of the prey matrix.

3.4.4 Marine Memory Saving

Marine predators possess the ability to remember successful foraging locations, and this characteristic is emulated through memory saving in the Marine Predator Algorithm (MPA). Once the Prey is updated and the FADs effect is implemented, the resulting matrix is evaluated for its fitness in order to update the Elite. The fitness of each solution in the current iteration is compared to its counterpart from the previous iteration, and if the current solution demonstrates better fitness, it replaces the previous one. This process ensures that the MPA retains the most fitting solutions over time.

Initialize search agents (Prey) populations i=1,....,n
While termination criteria are not met
Calculate the fitness and construct the Elite matrix
If Iter < IterMax
Update prey based on Eq.(3.7)
Else if IterMax/3 < Iter < 2*IterMax/3
For the first half of the populations (i=1,....,n/2)
Update prey based on Eq.(3.9)
For the other half of the populations (i = n/2,....,n)
Update prey based on Eq.(3.11)
Else if Iter > 2*IterMax /3
Update prey based on Eq.(3.13)
End (if)
Accomplish memory saving and Elite update
Applying FADs effect and update based on Eq. (3.14)
Accomplish memory saving and Elite update
End while

Figure 3.1: Pseudo code of the MPA approach

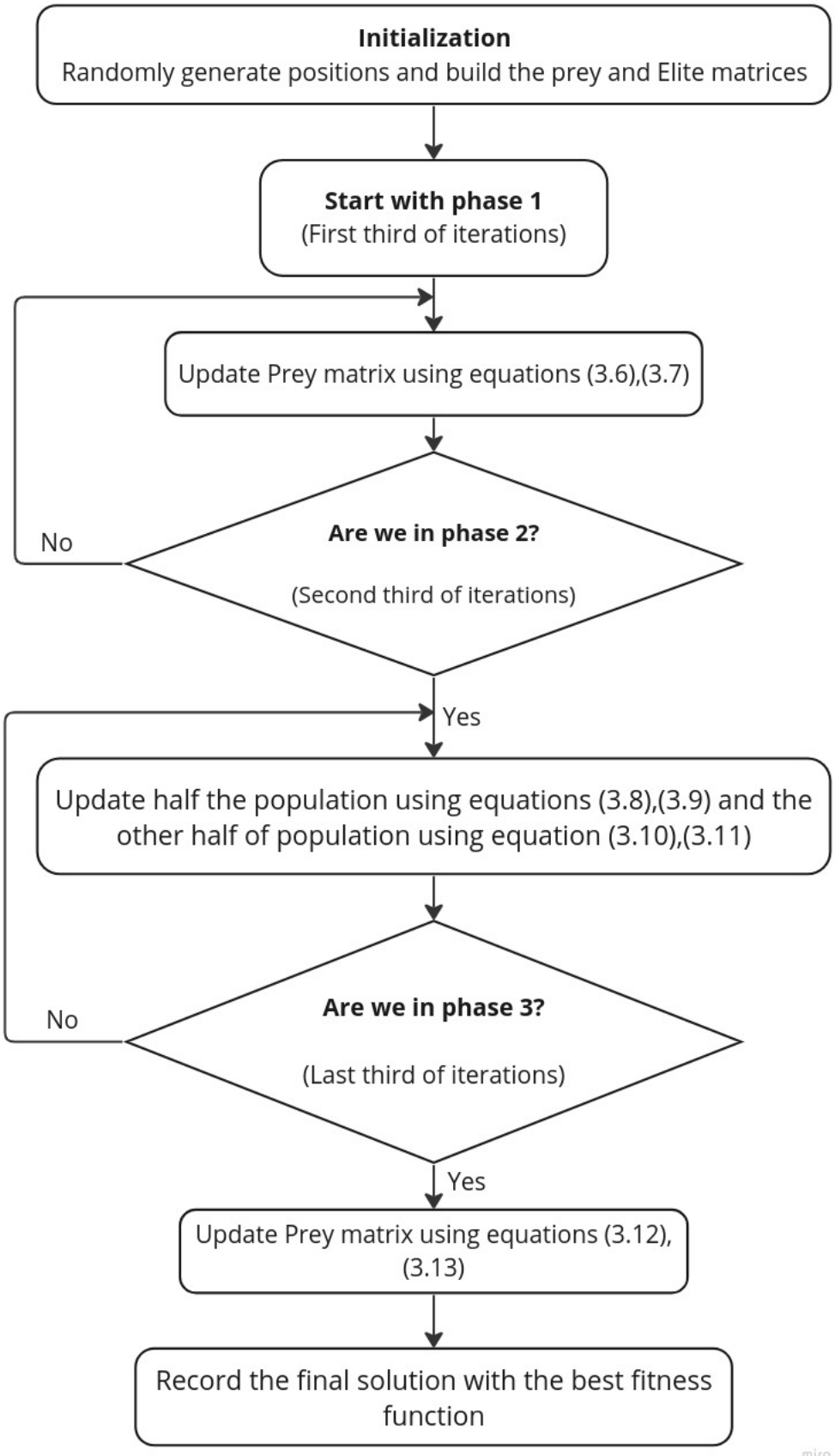

Figure 3.2: Flowchart for the Marine Predator Algorithm

3.5 Snake Optimizer Algorithm

The Snake Optimization Algorithm (SOA) is a metaheuristic algorithm inspired by the behavior of snakes in nature. It simulates the movement and hunting strategies of snakes to solve optimization problems.

3.5.1 Inspiration

The Snake Optimization (SO) algorithm draws inspiration from the mating behavior of snakes. The algorithm operates based on the availability of food and temperature conditions. The search process can be categorized into two phases, namely exploration and exploitation. During the exploration phase, snakes primarily focus on searching for food in their surroundings when environmental factors such as a cold place and food are absent.

The exploitation phase aims to achieve global optimization through several transitional phases. If food is available but the temperature is high, the snakes prioritize consuming the existing food. Conversely, when both food and a cold environment are present, the mating process is triggered. The mating process involves two distinct modes: fight mode and mating mode.

In the fight mode, male snakes compete to secure the best female partner, while females strive to select the most suitable male partner. In the mating mode, pairs of snakes mate based on the availability of food quantity. During the search process, there is a probability that females may lay eggs, which eventually hatch into new snakes, contributing to the exploration of the search space.

3.5.2 SOA Steps

1. **Initialization**
   Like all metaheuristics algorithms, SO starts by generating a random population in uniform distribution to be able to begin the optimization algorithm process. The initial population can be obtained using equation (3.2).

2. **Diving the swarm into two equal groups males and females**
   In this study, the number of male is assumed to be 50% and the number of females to be 50%. The population is divided to 2 groups: male group and female one. To divide the swarm use the following two Eqs. (3.15), (3.16).

$$N_m = N/2 \tag{3.15}$$

$$N_f = N - N_m \tag{3.16}$$

   where N is the number of individuals, N_m refers to the male individual numbers and N_f refers to the female individual numbers.

3. **Evaluating each group and defining temperature and food quantity**

   – Find the best individual in each group and get the best male ($f_{best,m}$) and best Female ($f_{best,f}$) and the Food position (f_{best}).

   – The Temperature $Temp$ can be defined using the following equation :

$$Temp = exp(\frac{-t}{T}) \tag{3.17}$$

   where t refers to the current iteration and T refers to the maximum number of iterations.

– Defining Food quantity (Q) The food quantity can be obtained using the following equation:

$$Q = c_1 * exp(\frac{t-T}{T}) \tag{3.18}$$

where c_1 is constant and equals 0.5.

4. **Exploration phase** (no food)
If Q < Threshold (Threshold = 0.25) the snakes search for food by selecting any random position and update their position respect to it. To model exploration phase the following equations are used :

$$X_{i,m}(t+1) = X_{rand,m}(t) \pm c_2 \times A_m \times ((X_{max} - X_{min}) \times rand + X_{min}) \tag{3.19}$$

where $X_{i,m}$ refers to ith male position,$X_{rand,m}$ refers to position of random male, $rand$ is a random number between 0 and 1, c_2 is constant and equals 0.05 and A_m is the male ability to find the food and can be calculated as follows:

$$A_m = exp(\frac{-f_{rand,m}}{f_{i,m}}) \tag{3.20}$$

where $f_{rand,m}$ is the fitness of $X_{rand,m}$ and $f_{i,m}$ is the fitness of ith individual in male group.

$$X_{i,f} = X_{rand,f}(t+1) \pm c_2 \times A_f \times ((X_{max} - X_{min}) \times rand + X_{min}) \tag{3.21}$$

where $X_{i,f}$ refers to ith female position,$X_{rand,f}$ refers to position of random female, $rand$ is a random number between 0 and 1 and A_f is the male ability to find the food and can be calculated as follows:

$$A_f = exp(\frac{-f_{rand,f}}{f_{i,f}}) \tag{3.22}$$

where $f_{rand,f}$ is the fitness of $X_{rand,f}$ and $f_{i,f}$ is the fitness of ith individual in female group.

5. **Exploitation phase** (food exists)
If Q > Threshold
If the temperature > Threshold (0.6)(hot)
The snakes will move to the food only.

$$X_{i,j}(t+1) = X_{food} \pm c_3 \times Temp \times rand \times ((X_{food} - X_{i,j}(t)) \tag{3.23}$$

where $X_{i,j}$ is the position of individual (male or female), X_{food} is the position of the best individuals, and c_3 is constant and equals 2.

If the temperature < Threshold (0.6)(cold)
The snake will be in the fight mode or mating mode.
Fight mode

$$X_{i,m}(t+1) = X_{i,m}(t) + c_3 \times FM \times rand \times ((Q \times X_{best,f} - X_{i,m}(t)) \tag{3.24}$$

where $X_{i,m}$ refers to ith male position, $X_{best,f}$ refers to the position of the best individual in female group, and FM is the fighting ability of male agent.

$$X_{i,f}(t+1) = X_{i,f}(t) + c_3 \times FF \times rand \times ((Q \times X_{best,m} - X_{i,f}(t)) \tag{3.25}$$

where $X_{i,f}$ refers to ith female position, $X_{best,m}$ refers to the position of the best individual in male group, and FF is the fighting ability of female agent. FM and FF can be calculated from the following equations:

$$FM = exp(\frac{-f_{best,f}}{f_i}) \tag{3.26}$$

$$FF = exp(\frac{-f_{best,m}}{f_i}) \tag{3.27}$$

where $f_{best,f}$ is the fitness of the best agent of female group, $f_{best,m}$ is the fitness of the best agent of male group, and f_i is the agent fitness.

Mating mode

$$X_{i,m}(t+1) = X_{i,m}(t) + c_3 \times M_m \times rand \times ((Q \times X_{i,f}(t) - X_{i,m}(t)) \tag{3.28}$$

$$X_{i,f}(t+1) = X_{i,f}(t) + c_3 \times M_f \times rand \times ((Q \times X_{i,m}(t) - X_{i,f}(t)) \tag{3.29}$$

where $X_{i,f}$ is the position of ith agent in female group and $X_{i,m}$ is the position of ith agent in male group and M_m&M_f refers to the mating ability of male and female respectively and they can be calculated as follow:

$$M_m = exp(\frac{-f_{i,f}}{f_{i,m}}) \tag{3.30}$$

$$M_f = exp(\frac{-f_{i,m}}{f_{i,f}}) \tag{3.31}$$

If Egg hatch, select worst male & Female and replace them

$$X_{worst,m} = X_{min} + rand(X_{max} - X_{min}) \tag{3.32}$$

$$X_{worst,f} = X_{min} + rand(X_{max} - X_{min}) \tag{3.33}$$

where $X_{worst,m}$ is the worst individual in male group, $X_{worst,m}$ is the worst individual in female group. The flag direction operator which is also called diversity factor, gives possibility to increase or decrease positions' solution to give high opportunities to change the direction of agents that results a good scan of the given search space in all possible directions. This parameter generated randomly to achieve randomization aspect hat is essential in any metaheuristic algorithm.

The process will continue for a number of iteration from step 2, if the criterion is satisfied the process will be terminated[26].

Initialize Problem Setting (Dim ,Ub, Lb, and Popsize(N),MaxIter(T),CurrIter(t))

Initialize the population randomly

Divide population into 2 equal groups N_m and N_f using Eqs.(3.15) and (3.16)

While(t $\leq$ T) do

Evaluate each group N_m and N_f

Find best male $f_{best,m}$

find best female $f_{best,f}$

Define Temp using Eq.(3.17)

Define food quantity Q using Eq. (3.18)

If (Q $<$ 0.25) then
Perform exploration using Eqs; (3.19) and (3.21)

Else if (Q $>$ 0.6) then
Perform exploitation Eq. (3.23)

Else
If (rand $>$ 0.6) then
Snakes in Fight mode Eqs. (3.24) and (3.25)

Else
Snakes in Mating Mode Eqs. (3.28) and (3.29)
Change the worst male and female Eqs. (3.32) and (3.33)
End if
End if
End while

Return best solution

Figure 3.3: Pseudo code of the SOA approach

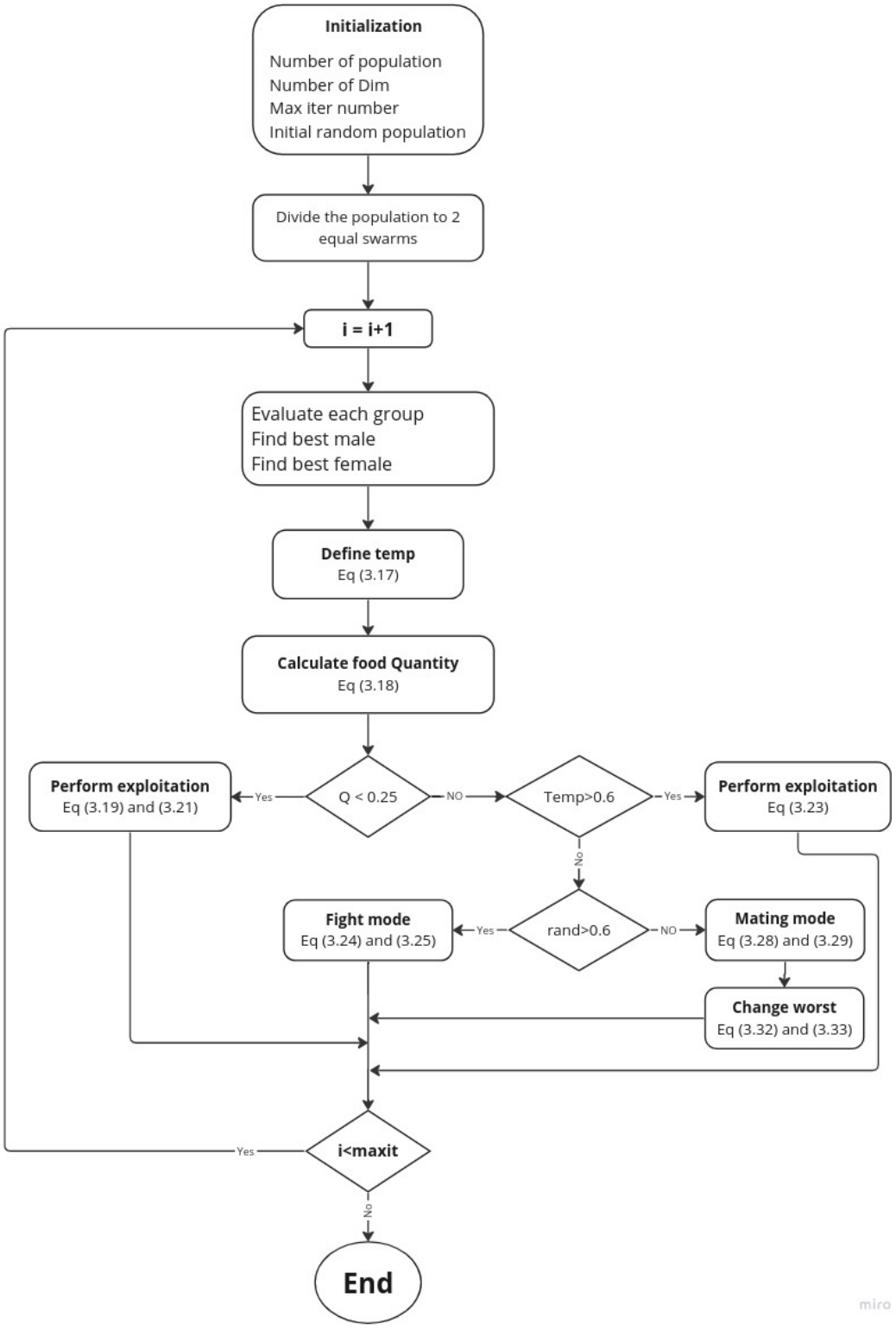

Figure 3.4: Flowchart for the Snake Optimizer Algorithm

3.6 Conclusion

In mathematics, optimization is defined as finding the best solution for a problem from all feasible solutions [33]. Depending on whether the variables are continuous or discrete, the process of finding values of variables that satisfy an objective function is called optimization. In this chapter, two of the optimization algorithms which are MPA and SOA were demonstrated, with a discussion of their approaches of search. The algorithms were used to minimize the objective function in order the extract the needed parameters of the Bifacial cell model. The last chapter will present the results of this process and discuss them.

Chapter Four : Results and Discussions

4.1 Introduction

In this section, the results of MPA based bifacial PV single-diode model parameters extraction are shown for five different levels of irradiation to observe their effect on the bifacial technology.The provided data are I-V characteristics of bifacial (PERC) single-cell laminate in its reference state at five irradiation levels ranging from 185 W/m^2 to 925 W/m^2 (I_f-V and I_r-V measurements). The results consist of I-V and depicting both estimated and measured current data, P-V curves presenting both estimated and measured power, and graphs showing the modified RMSE vs iteration number. Also a small comparison is done between MPA,SOA and Particle swarm Optimization (PSO) and Differentiel Evolution (DE) algorithms.
The algorithms used are population-based ones, Here is the way they were used :

- The number of iterations and number of population are chosen.
  As a rule of thumb, since the number of parameters is ten, the number of population is chosen to be ten times that number (number of population=100). The maximum number of iterations is chosen to be 1000.
- Algorithm coefficients are initialized; these coefficients can be tuned along the program depending on the algorithm.
- A random initial population is initialized within the parameters boundaries. Each population member is a vector of the ten parameters of interest:
  v=$[a_f, I_{0f}, I_{phf}, R_{pf}, R_{sf}, a_r, I_{0r}, I_{phr}, R_{pr}, R_{sr}]$

Parameter	search range
a_f	[1, 2]
I_{0f}	[1µA, 5µA]
I_{phf}	$[0.95 \times I_{scf}\ ,\ 1.05 \times I_{scf}\ ]$
R_{pf}	$[\frac{V_{mppf}}{I_{scf}-I_{mppf}}, 1000\Omega]$
R_{sf}	$[0\ ,\ \frac{V_{mppf}-V_{ocf}}{I_{mppf}}]$
a_r	[1, 2]
I_{0r}	[1µA, 5µA]
I_{phr}	$[0.95 \times I_{scr}\ ,\ 1.05 \times I_{scr}\ ]$
R_{pr}	$[\frac{V_{mppr}}{I_{scr}-I_{mppr}}, 1000\Omega]$
R_{sr}	$[0\ ,\frac{V_{mppr}-V_{ocr}}{I_{mppr}}]$

Table 4.1: SDM Parameter search ranges

- Population members are updated; with the boundary conditions checked and respected, in order to get a better modified RMSE.
- The fitness (modified RMSE) of each population member (candidate solution) is evaluated.
- The algorithms run for a defined number of iterations and give the smallest obtained value of the modified RMSE.

4.2 Results

In this section, the results of SOA and MPA based PV single-diode model parameters extraction are shown. The results consist of I-V curves depicting both estimated and measured current data, and graphs showing the convergence curve of each algorithm. The results are organised as follows:

- Each algorithm has four results sections (for the five different irradiance levels)
- Each section comprises two graphs: modified RMSE vs iteration and I-V curve

4.2.1 Parameters Identification Using MPA

Case study #1 : G=925W/m^2

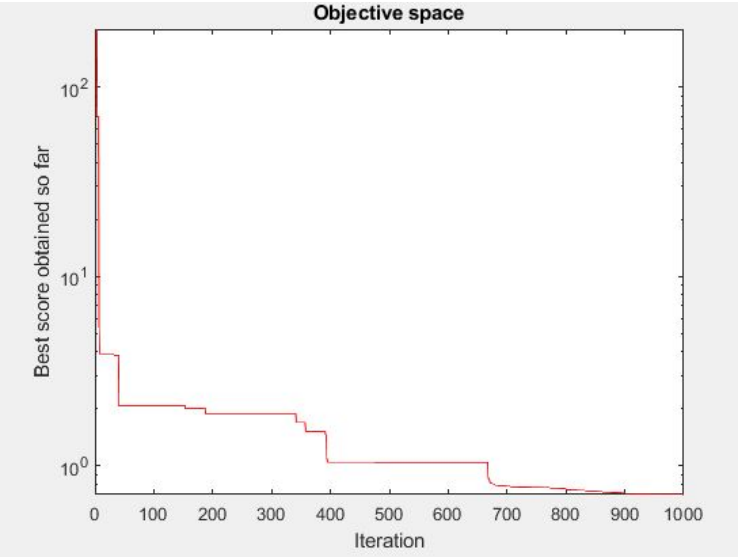

Figure 4.1: Convergence curve of the MPA on a PERC bifacial cell at G=925W/m^2

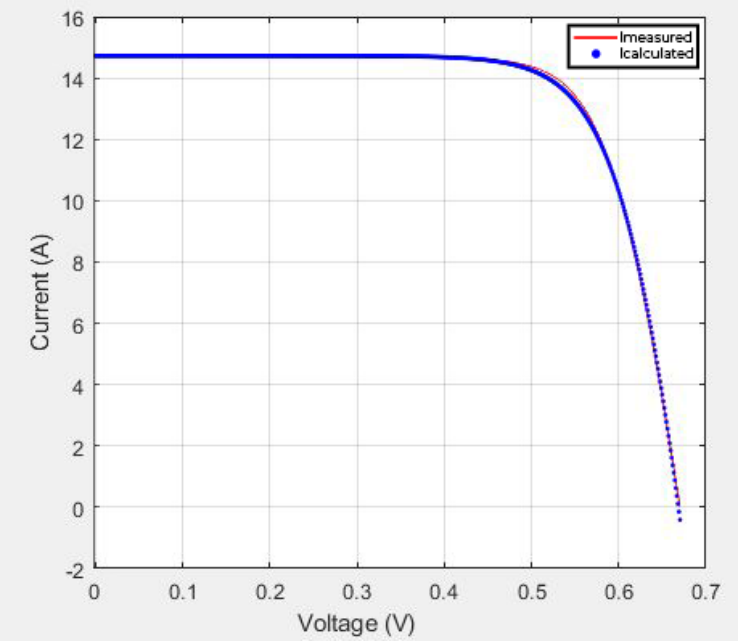

Figure 4.2: I-V Curve of both calculated (through MPA) and measured currents at G=925W/m^2

Case study #2 : G=740W/m^2

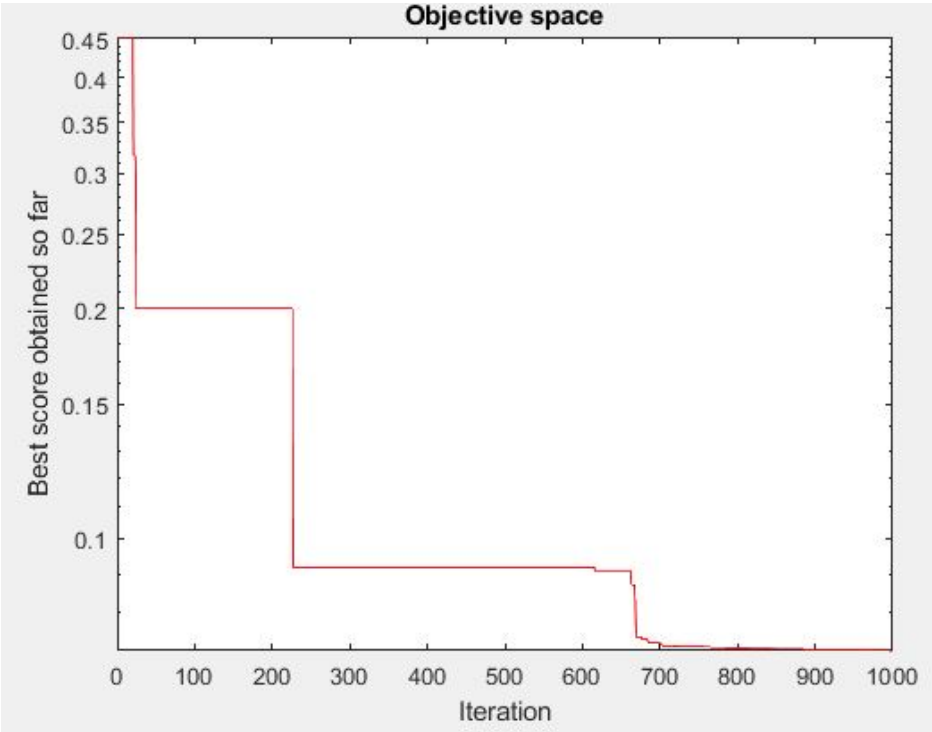

Figure 4.3: Convergence curve of the MPA on a PERC bifacial cell at G=740W/m^2

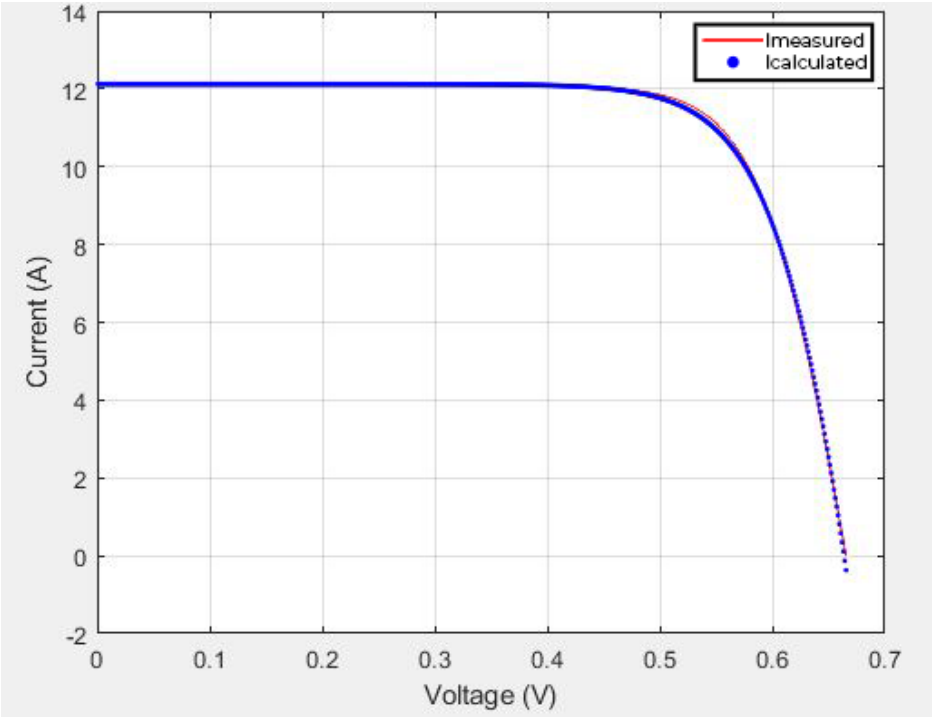

Figure 4.4: I-V Curve of both calculated (through MPA) and measured currents at G=740W/m^2

Case study #3 : G=555W/m^2

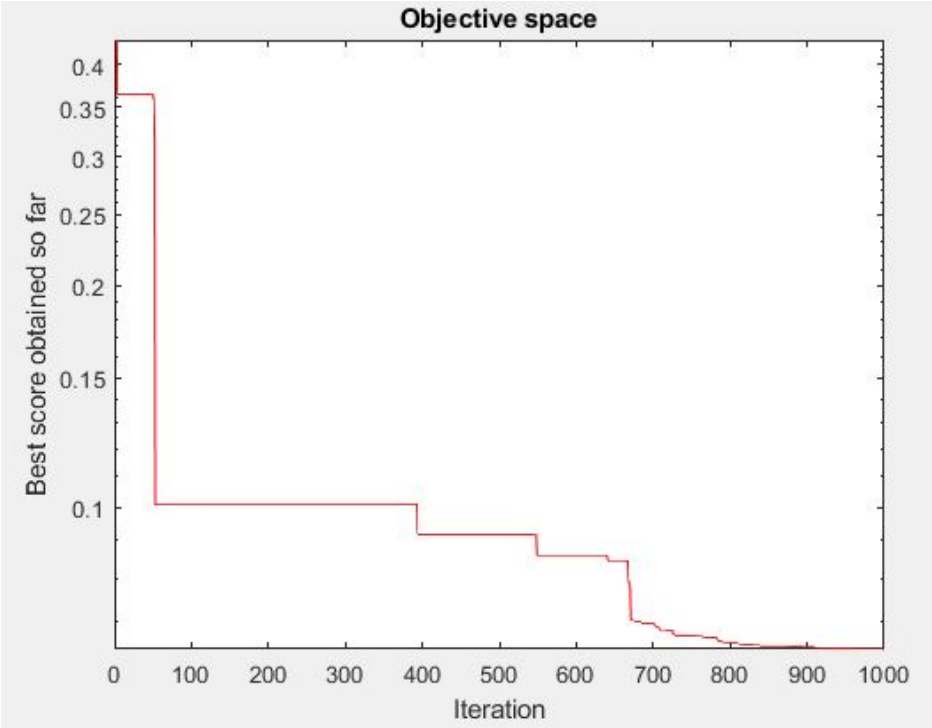

Figure 4.5: Convergence curve of the MPA on a PERC bifacial cell at G=555W/m^2

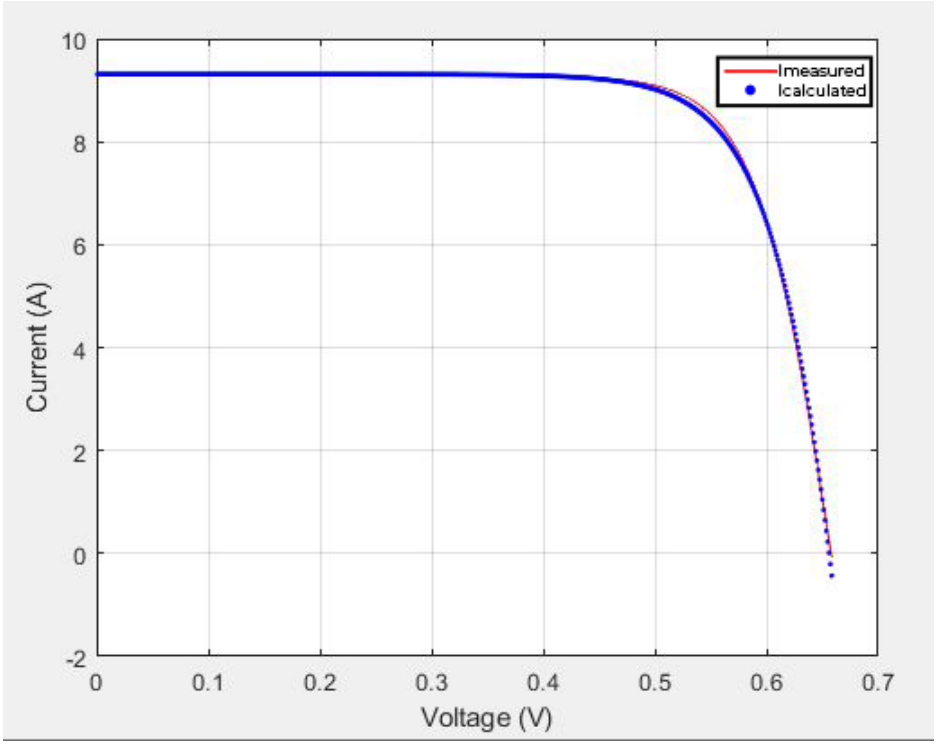

Figure 4.6: I-V Curve of both calculated (through MPA) and measured currents at G=555W/m^2

Case study #4 : G=370W/m^2

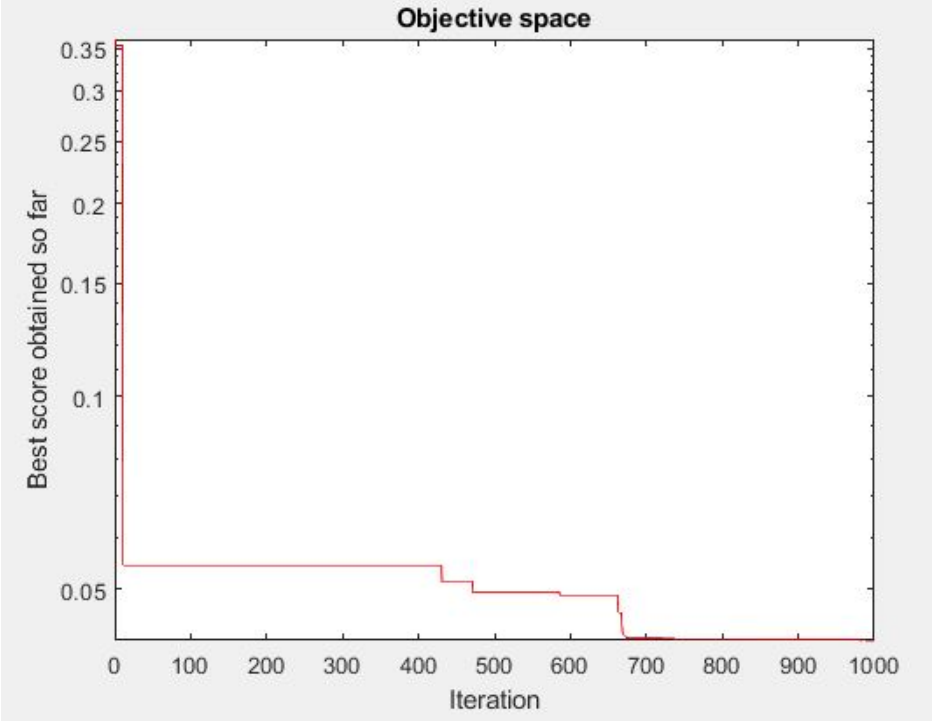

Figure 4.7: Convergence curve of the MPA on a PERC bifacial cell at G=370W/m^2

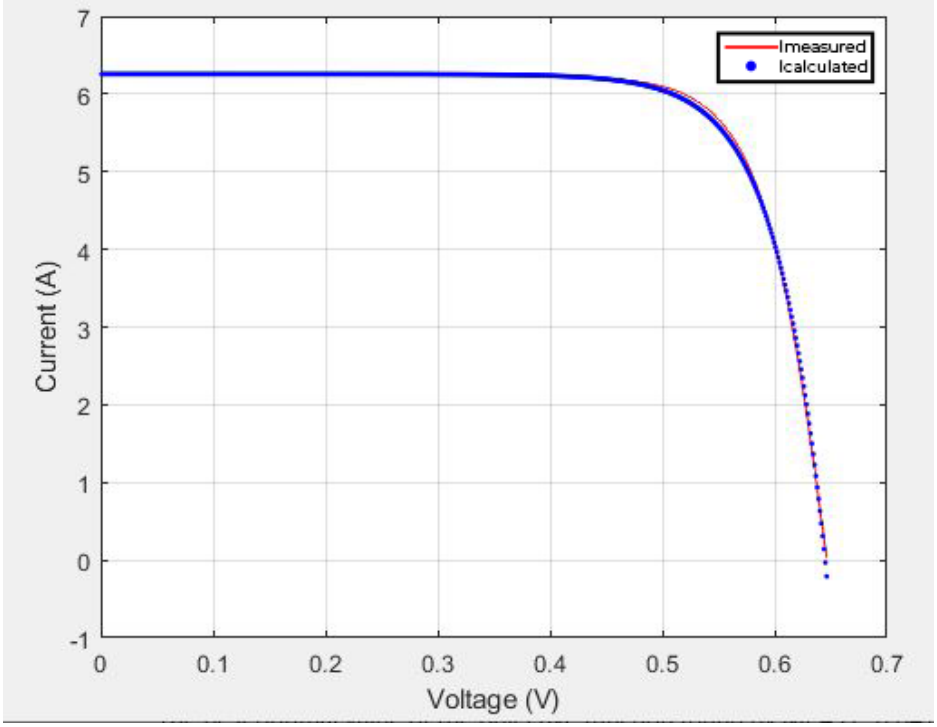

Figure 4.8: I-V Curve of both calculated (through MPA) and measured currents at G=370W/m^2

Case study #5 : G=185W/m^2

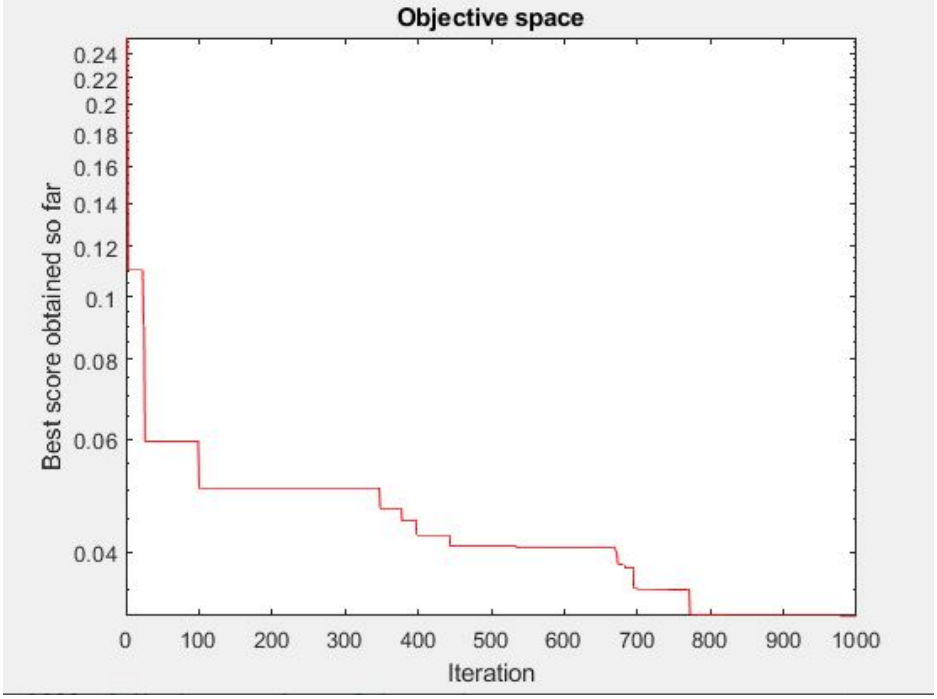

Figure 4.9: Convergence curve of the MPA on a PERC bifacial cell at G=185W/m^2

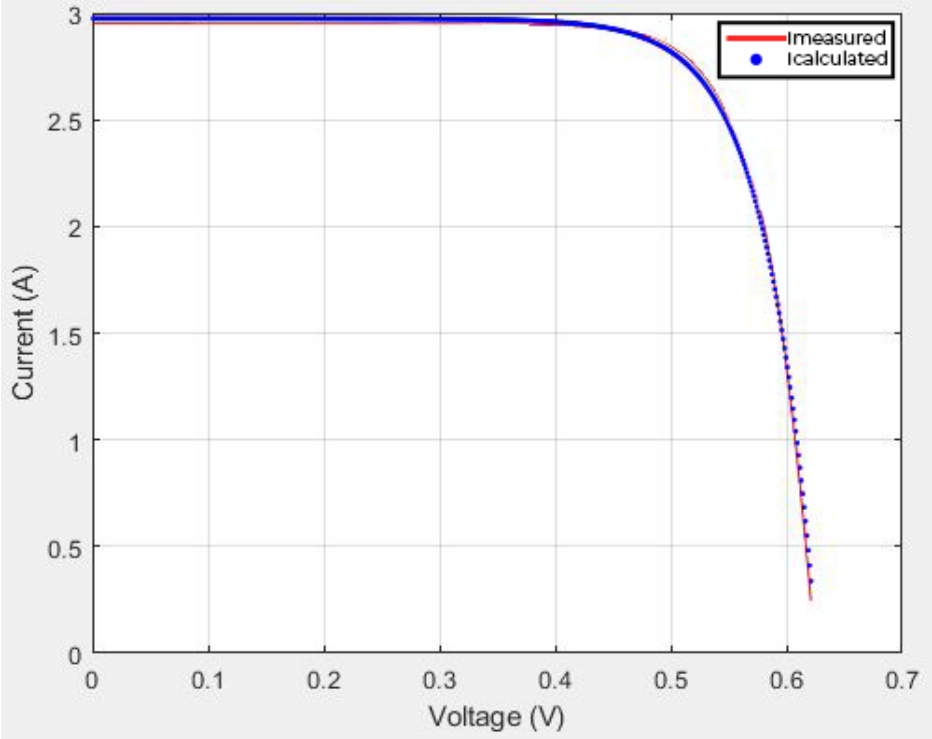

Figure 4.10: I-V Curve of both calculated (through MPA) and measured currents at G=185W/m^2

Parameters	G=925W/m^2	G=740W/m^2	G=555W/m^2	G=370W/m^2	G=185W/m^2
a_f	1.541177328	1.546026969	1.558499924	1.565593841	1.597997258
I_{0f}	1.000192e-06	1.017646846e-06	1.00044e-06	1.0007e-06	1.0001e-06
I_{phf}	8.153356626	7.118371666	5.38097546	3.650015015	1.751312501
R_{pf}	225.0685395	281.6685674	376.042325	563.7715687	1128.342699
R_{sf}	0.00800235	0.00805009	0.0080039	0.0080258	0.00801276
a_r	2	2	2	2	2
I_{0b}	1e-06	1e-06	1e-06	1e-06	1e-06
I_{phr}	6.636685015	5.007618179	3.929697255	2.606081068	1.222243235
R_{pr}	242.418856	303.13357	404.8413266	606.18724	1212.23427
R_{sr}	0.008511	0.008763	0.0089201	0.008982	0.0093716
RMSE	0.07664587929	0.07140995982	0.0616539666	0.04157017744	0.03181410063

Table 4.2: The extracted model parameters using MPA

4.2.2 Parameters Identification Using SOA

Case study #1 : G=925W/m^2

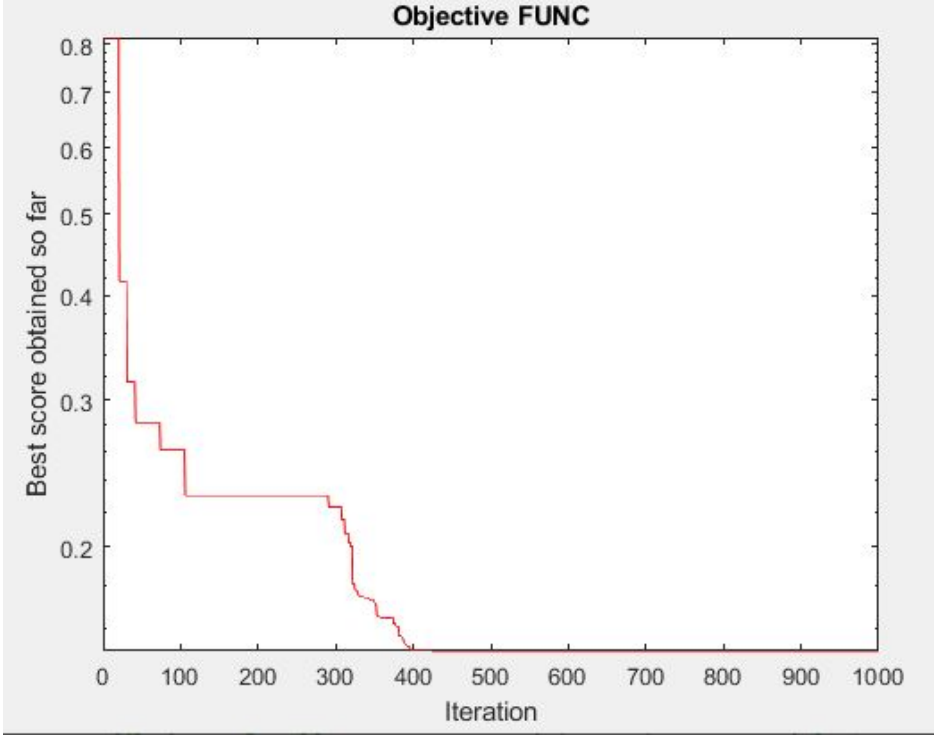

Figure 4.11: Convergence curve of the SOA on a PERC bifacial cell at G=925W/m^2

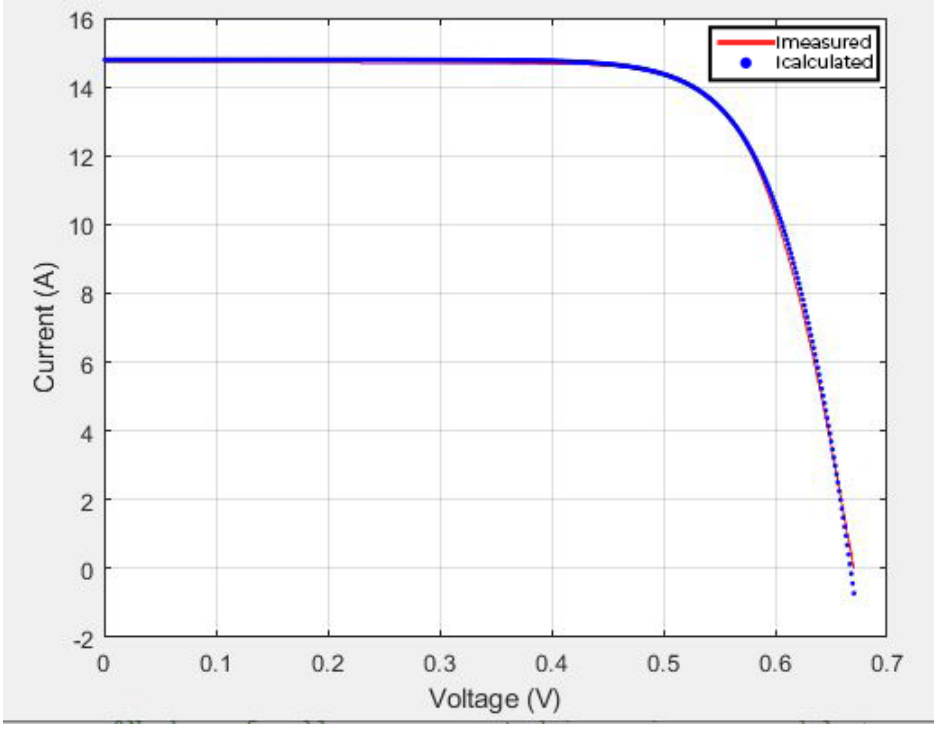

Figure 4.12: I-V Curve of both calculated (through SOA) and measured currents at G=925W/m^2

Case study #2 : G=740W/m^2

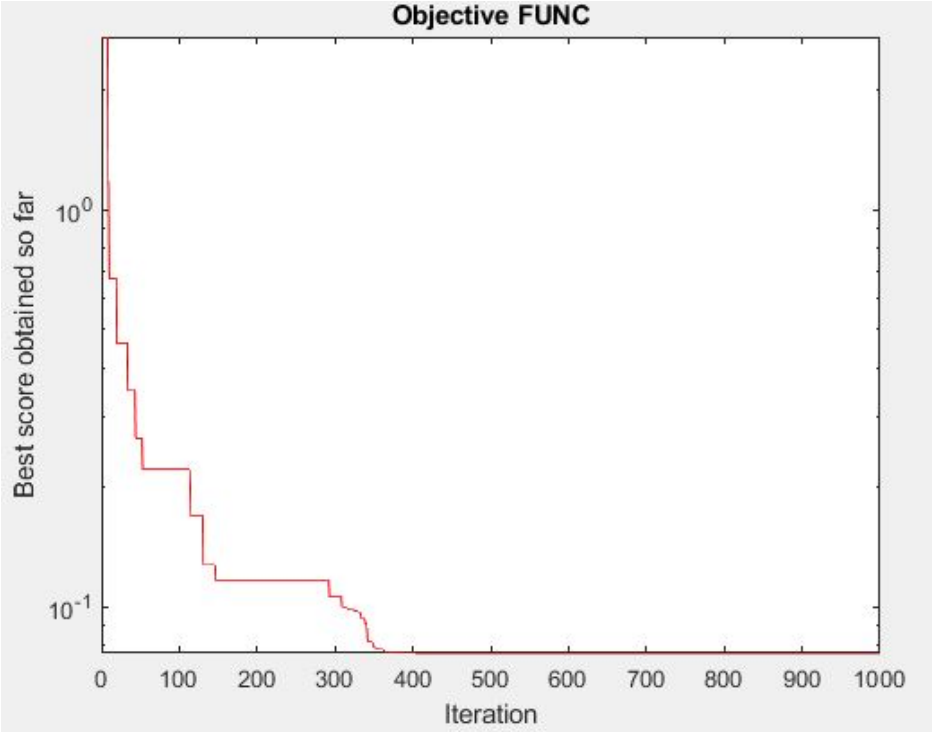

Figure 4.13: Convergence curve of the SOA on a PERC bifacial cell at G=740W/m^2

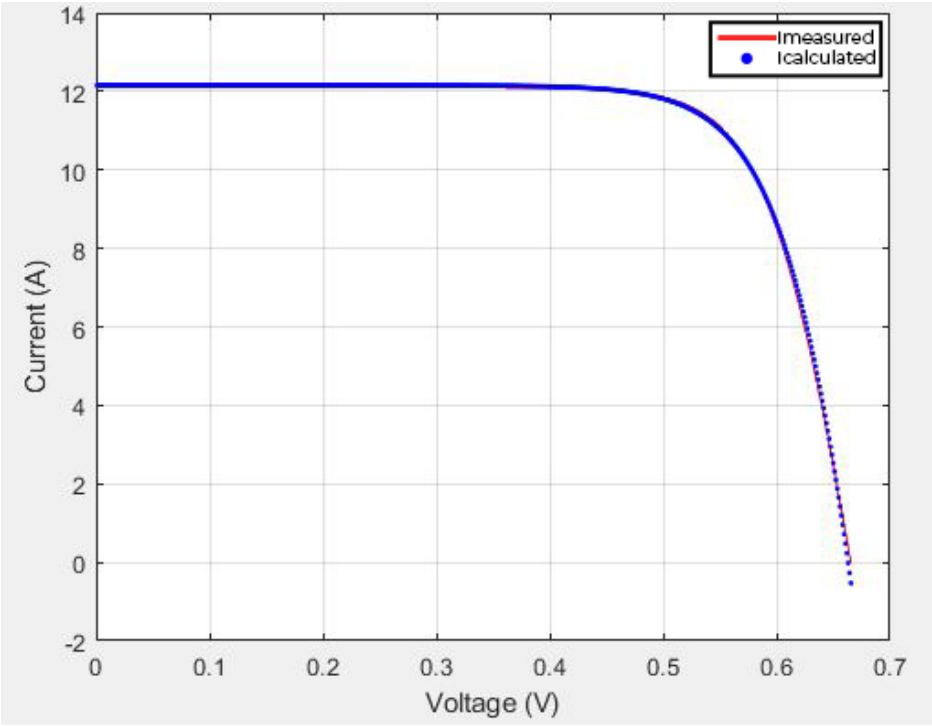

Figure 4.14: I-V Curve of both calculated (through SOA) and measured currents at G=740W/m^2

Case study #3 : G=555W/m^2

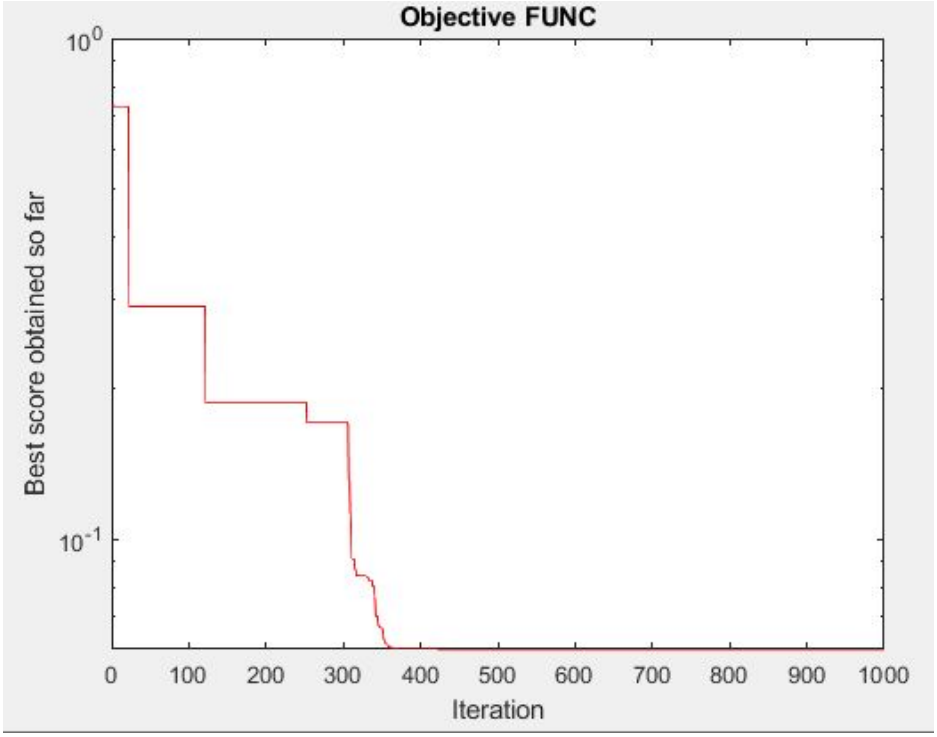

Figure 4.15: Convergence curve of the SOA on a PERC bifacial cell at G=555W/m^2

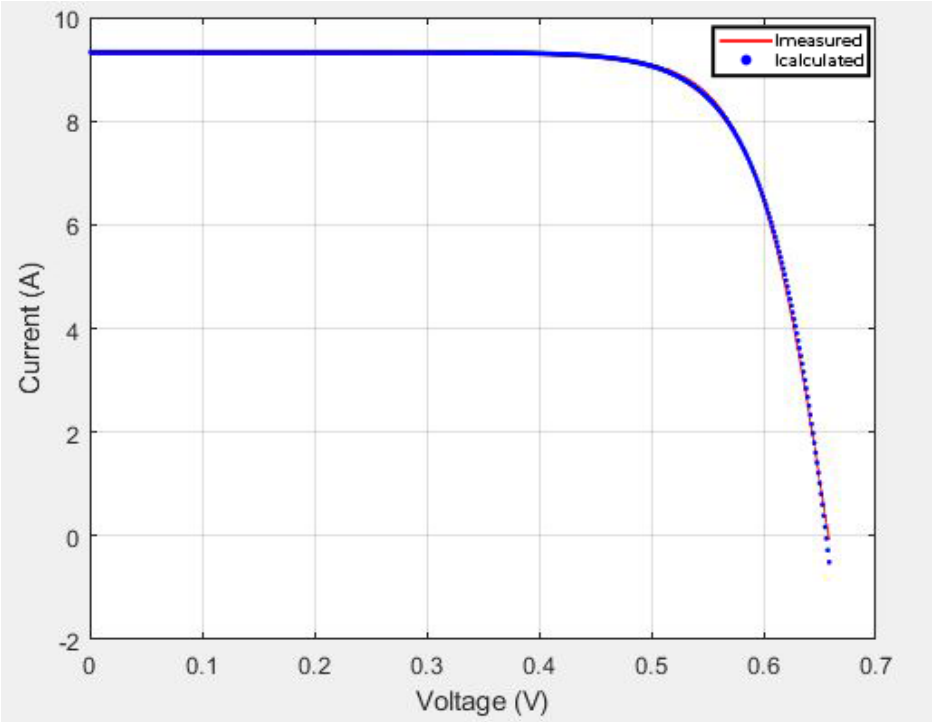

Figure 4.16: I-V Curve of both calculated (through SOA) and measured currents at G=555W/m^2

Case study #4 : G=370W/m^2

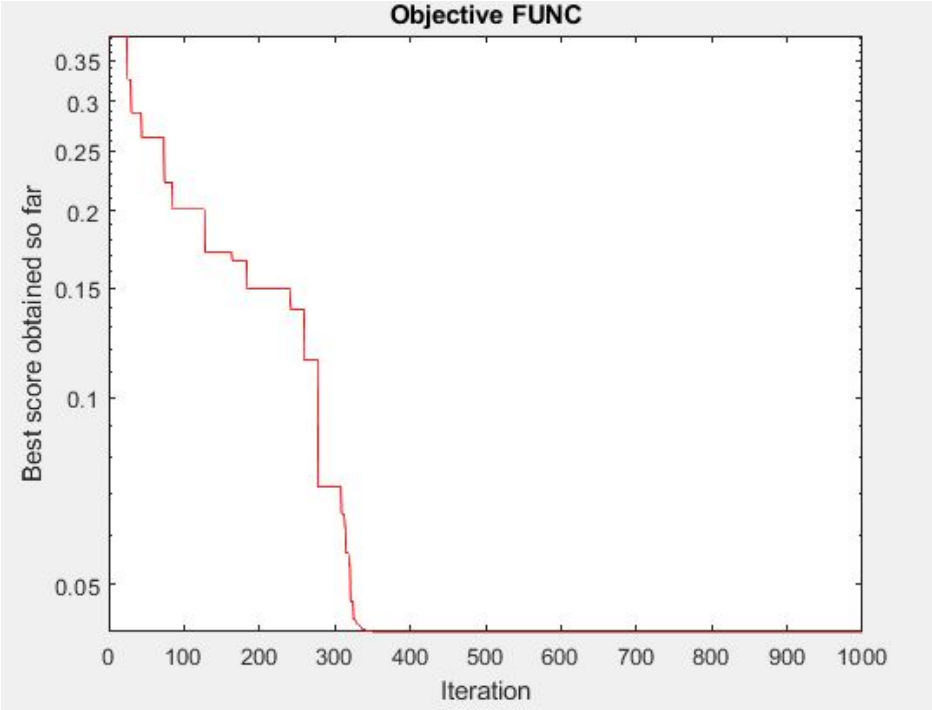

Figure 4.17: Convergence curve of the SOA on a PERC bifacial cell at G=370W/m^2

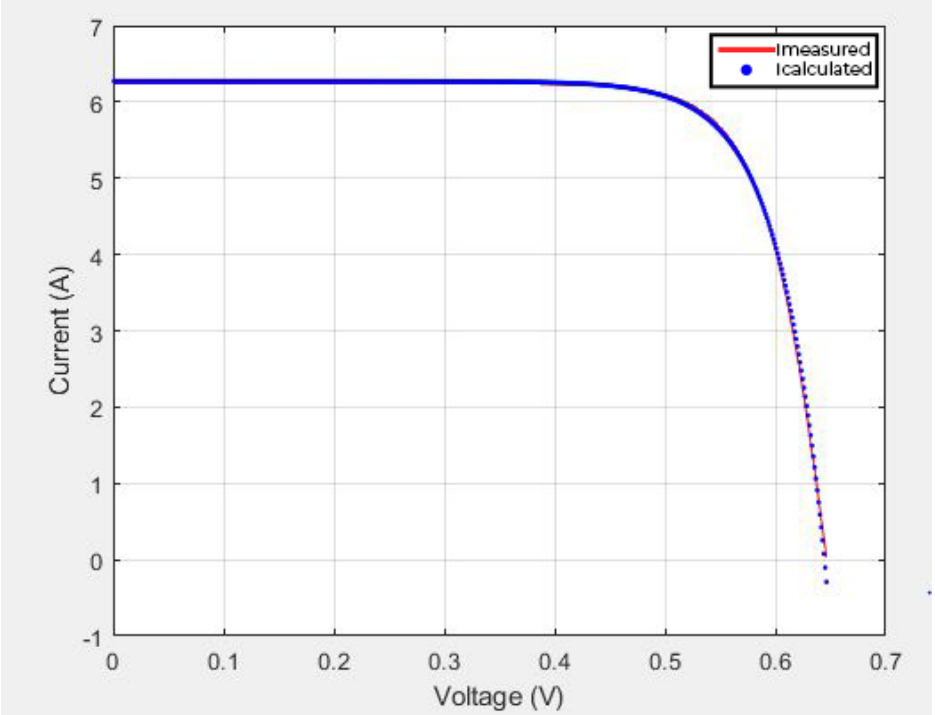

Figure 4.18: I-V Curve of both calculated (through SOA) and measured currents at G=370W/m^2

Case study #5 : G=185W/m^2

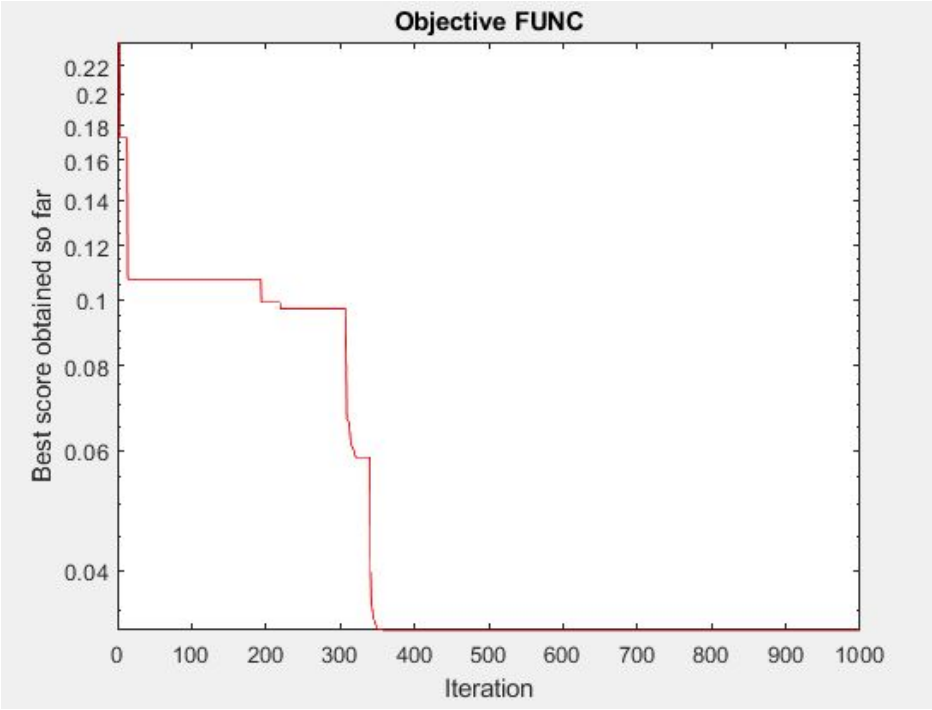

Figure 4.19: Convergence curve of the SOA on a PERC bifacial cell at G=185W/m^2

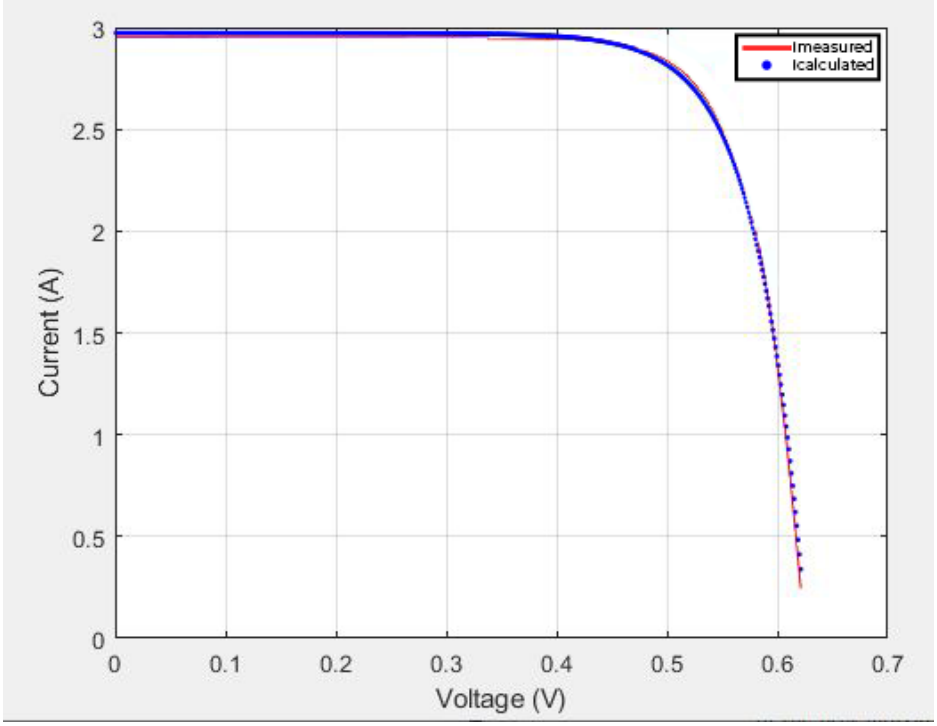

Figure 4.20: I-V Curve of both calculated (through SOA) and measured currents at G=185W/m^2

Parameters	G=925W/m^2	G=740W/m^2	G=555W/m^2	G=370W/m^2	G=185W/m^2
a_f	1.537205875	1.544571639	1.552530755	1.564558772	1.59800601
I_{0f}	1e-06	1e-06	1e-06	1e-06	1e-06
I_{phf}	8.186910155	7.18797	5.110252663	3.40953893	1.623678845
R_{pf}	230.106427	292.4330447	388.011712	582.668073	1166.623426
R_{sf}	0.0080635	0.00809241	0.008132	0.0081279	0.0081287
a_b	2	2	2	2	2
I_{0b}	1e-06	1e-06	1e-06	1e-06	1e-06
I_{phb}	6.541098615	5.202882681	4.199005356	2.84320683	1.342805383
R_{pf}	249.9643728	311.544577	416.728860	624.510344	1250.679128
R_{sb}	0.008517472	0.00870841972	0.00894958	0.0089963	0.009163
RMSE	0.0895808753	0.07630082773	0.06017209404	0.04197653735	0.03274338952

Table 4.3: The extracted model parameters using SOA

4.3 Discussion

The employed algorithms have demonstrated excellent performance, as evidenced by the low estimated error values obtained. This indicates that the variance between the experimental and calculated data is minimal, reflecting the accuracy of the extracted parameters. Consequently, the established models can be deemed reliable and effectively represent the modules. A visual examination of the resulting I-V curves further confirms the accuracy of the models, as the calculated data points closely align with the experimental curves.

The convergence curves, which depict the relationship between the number of iterations and the convergence behavior of the five algorithms, provide insights into their performance in searching for optimal parameter values to achieve the lowest possible estimated error. It can be observed that the algorithms exhibit consistent patterns during the optimization process. For instance, the curve for MPA displays a staircase-like behavior, indicating a gradual descent of the estimated error values in relatively large steps. Another notable observation is that the majority of the curves demonstrate that the best error value is attained well before reaching the predetermined maximum number of iterations. Therefore, there is no need to increase the iteration count in search of further improvements.

Demonstrating the irradiance effect on the extracted parameters

- The series resistance is a critical parameter that can negatively impact the power output and fill factor of a photovoltaic (PV) module, using both algorithms the series resistance is independent of irradiance.

$$R_{sf}(G,T) \approx R_{sfSTC} \tag{4.1}$$

$$R_{sb}(G,T) \approx R_{sbSTC} \tag{4.2}$$

- The shunt resistance models the p-n junction non-idealities and its effect is equivalent to partial short-circuiting at the junction, which reduces the output current,it varies inversely with irradiance.

$$R_{pf}(G,T) \approx (\frac{G_{STC}}{G})R_{pfSTC} \tag{4.3}$$

$$R_{pr}(G,T) \approx (\frac{G_{STC}}{G})R_{prSTC} \tag{4.4}$$

- The photocurrent is known to be a strong function of irradiance, since it refers to the electric current generated by the absorption of light. As the irradiance increases the current eventually increases.

$$I_{phf}(G,T) \approx (\frac{G}{G_{STC}})I_{phfSTC} \tag{4.5}$$

$$I_{phr}(G,T) \approx (\frac{G}{G_{STC}})I_{phrSTC} \tag{4.6}$$

Through rigorous experimentation and analysis, a strong alignment was observed between the extracted parameters and the equations above under different irradiation levels. This compatibility reaffirms the robustness and reliability of the used algorithms in accurately estimating the PV system parameters, even when subjected to varying irradiation conditions.
The consistent agreement between the obtained results and the mentionned equations highlights the algorithms ability to capture the complex relationship between the PV system parameters and their response to changes in irradiation. This valuable insight enhances our understanding of the underlying principles governing PV systems and their behavior under different irradiation levels.

Comparative Discussion

Among the numerous optimization algorithms available, two widely utilized and well-established approaches for parameter identification are Particle Swarm Optimization (PSO) and Differential Evolution (DE). These algorithms have demonstrated their effectiveness and efficiency in tackling the challenging task of parameter identification in various domains. In order to check the used algorithms efficiency we have applied both PSO and DE on the studied SDM model.

- PSO Results

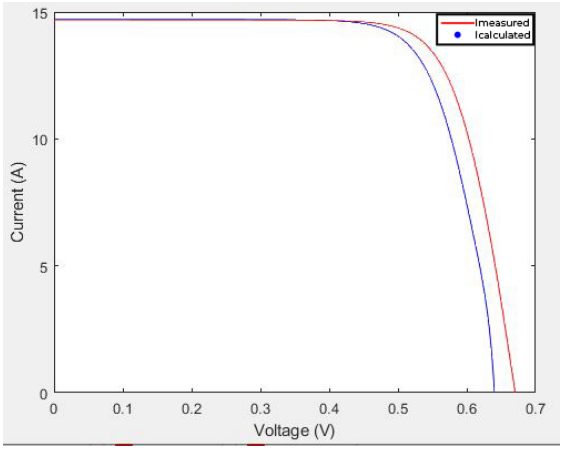

(a) I-V Curve of both calculated (through PSO) and measured currents at G=925W/m^2

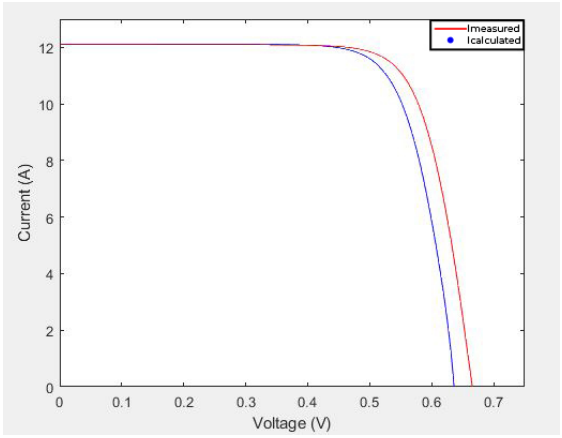

(b) I-V Curve of both calculated (through PSO) and measured currents at G=740W/m^2

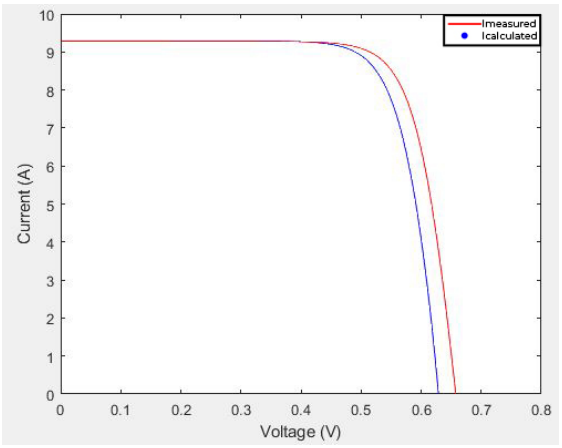

(c) I-V Curve of both calculated (through PSO) and measured currents at G=555W/m^2

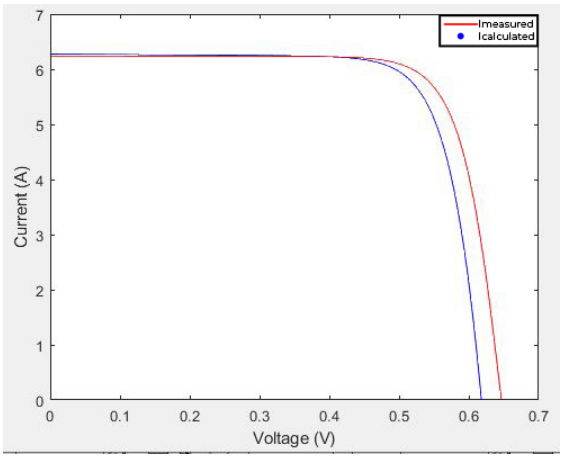

(d) I-V Curve of both calculated (through PSO) and measured currents at G=370W/m^2

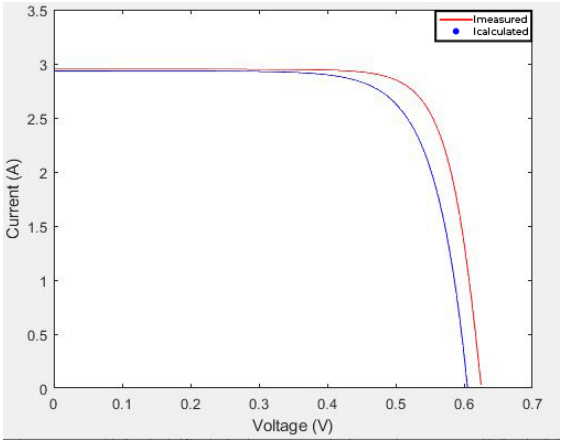

(e) I-V Curve of both calculated (through PSO) and measured currents at G=185W/m^2

- DE Results

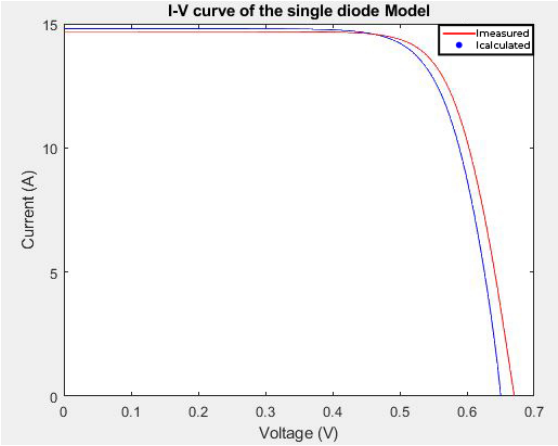

(a) I-V Curve of both calculated (through DE) and measured currents at G=925W/m^2

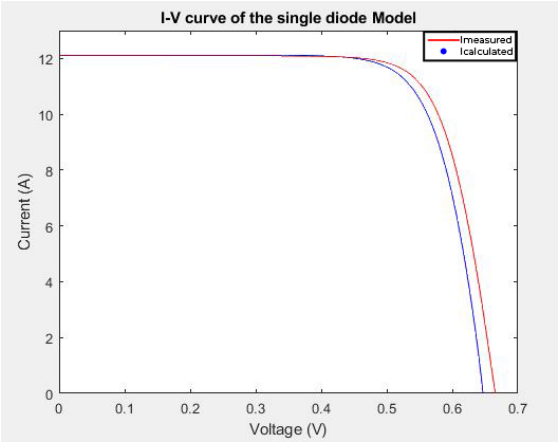

(b) I-V Curve of both calculated (through DE) and measured currents at G=740W/m^2

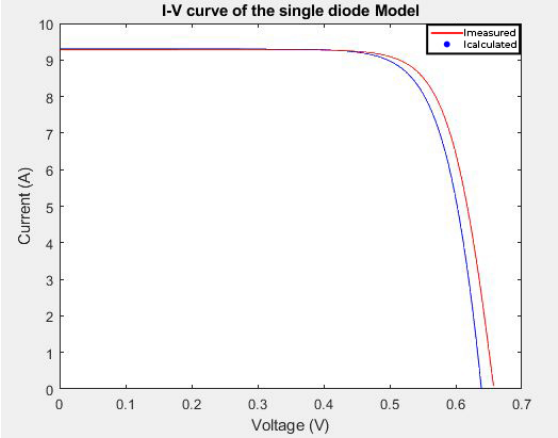

(c) I-V Curve of both calculated (through DE) and measured currents at G=555W/m^2

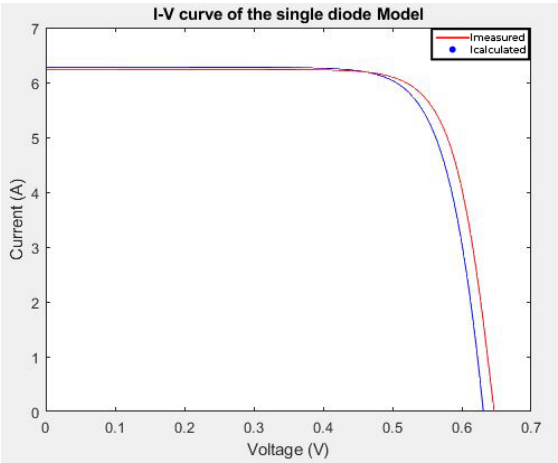

(d) I-V Curve of both calculated (through DE) and measured currents at G=370W/m^2

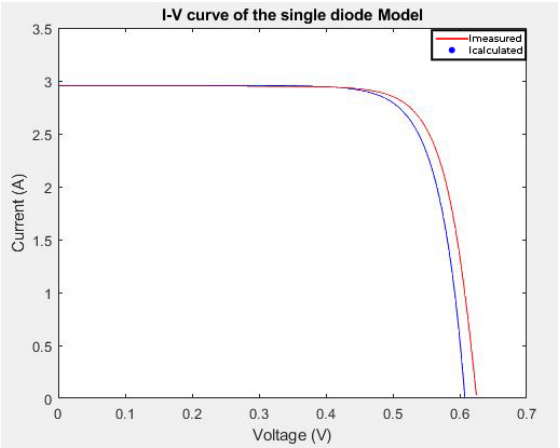

(e) I-V Curve of both calculated (through DE) and measured currents at G=185W/m^2

Algorithm	G=925W/m^2	G=740W/m^2	G=555W/m^2	G=370W/m^2	G=185W/m^2
MPA	7.664587929e-2*	7.140995982e-2*	6.16539666e-2	4.157017744e-2*	3.181410063e-2*
SOA	8.95808753e-2	7.630082773e-2	6.017209404e-2*	4.197653735e-2	3.274338952e-2
PSO	1.56060e-1	1.52509e-1	1.69996e-1	1.68952e-1	1.94069e-1
DE	1.2753e-1	1.2698e-1	1.291e-1	1.387e-1	1.26374e-1

Table 4.4: Comparative table of the error values of the five irradiation for MPA,SOA, PSO and DE

*: best obtained error value for the module.

From the comparative tables above, MPA is clearly on top in terms of error values; it has four best error values out of four. It has not even reached a value above 0.08; this shows the effectiveness of this optimization method for the purpose of single-diode model PV parameters extraction. SOA has also given one best results, which shows that this newly developed algorithm is very effective.
The widely used algorithms (PSO and DE) did not give the desired results ,as shown on the five I-V curves corresponding to their simulation,the difference between the simulated current and the experimental one were clearly obvious. The smallest error at both PSO and DE was still higher than the worst error on MPA and SOA.

Another observation is the narrow gap in error values overall between MPA and SOA; the gap is very narrow between the two values on all the table.
The widely varying parameter, between the algorithms results, are the parallel resistances R_{pf} and R_{pr}; this is mainly due to its wider range.
The less varying parameter between the two algorithms results is the photo-generated current I_{phf} and I_{phr}; this is logical because I_{phf} and I_{phr} must be very close to the short-circuit current of the module.

Proposed Objective Function Effect

In order to obtain the best results as mentionned previously we used a modified version of RMSE , to observe the effect of this edit on the parameters obtained we have plotted the error between the measured and the simulated currents calculated from both usual RMSE and the modified one versus voltage .

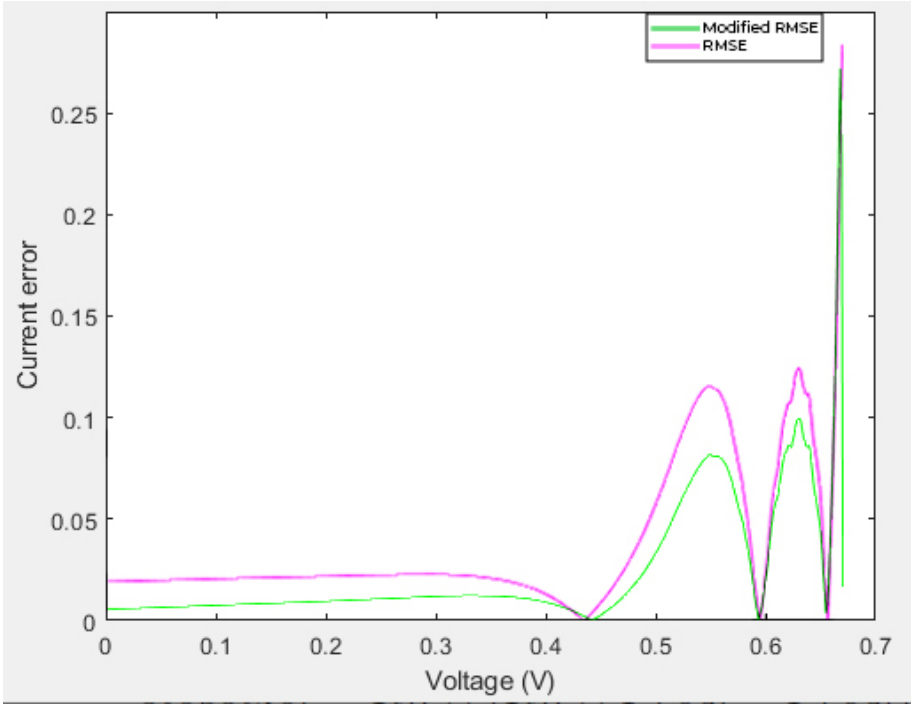

Figure 4.23: Current error of both RMSE and modified RMSE at G = 925 W/m^2

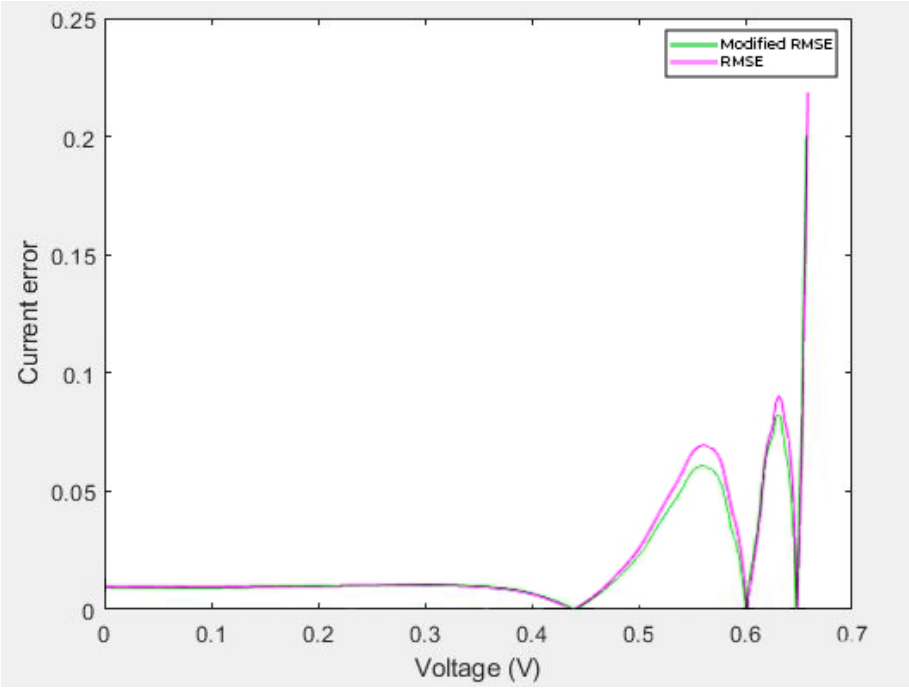

Figure 4.24: Current error of both RMSE and modified RMSE at G = 555 W/m^2

As we can see the error obtained from the modified RMSE is noticeably less than the one obtained from the regular RMSE especially around the maximum power point voltage .

4.4 SDM Model Simulation

The primary objective of parameter identification is to achieve precise determination of the model parameters that effectively characterize the behavior of the bifacial photovoltaic (PV) cell. The accuracy and reliability of this technique heavily rely on the alignment between model predictions and observed experimental data. To demonstrate the efficacy of the parameter identification process, a SIMULINK circuit was constructed to represent the single-diode model (SDM), utilizing the parameter values obtained from the results of the Marine Predators algorithm.

In order to assess the performance of the SDM model, a simulation was conducted at a specific irradiance level of G = 925 W/m^2. The Simulink circuit is depicted in Fig 4.21.

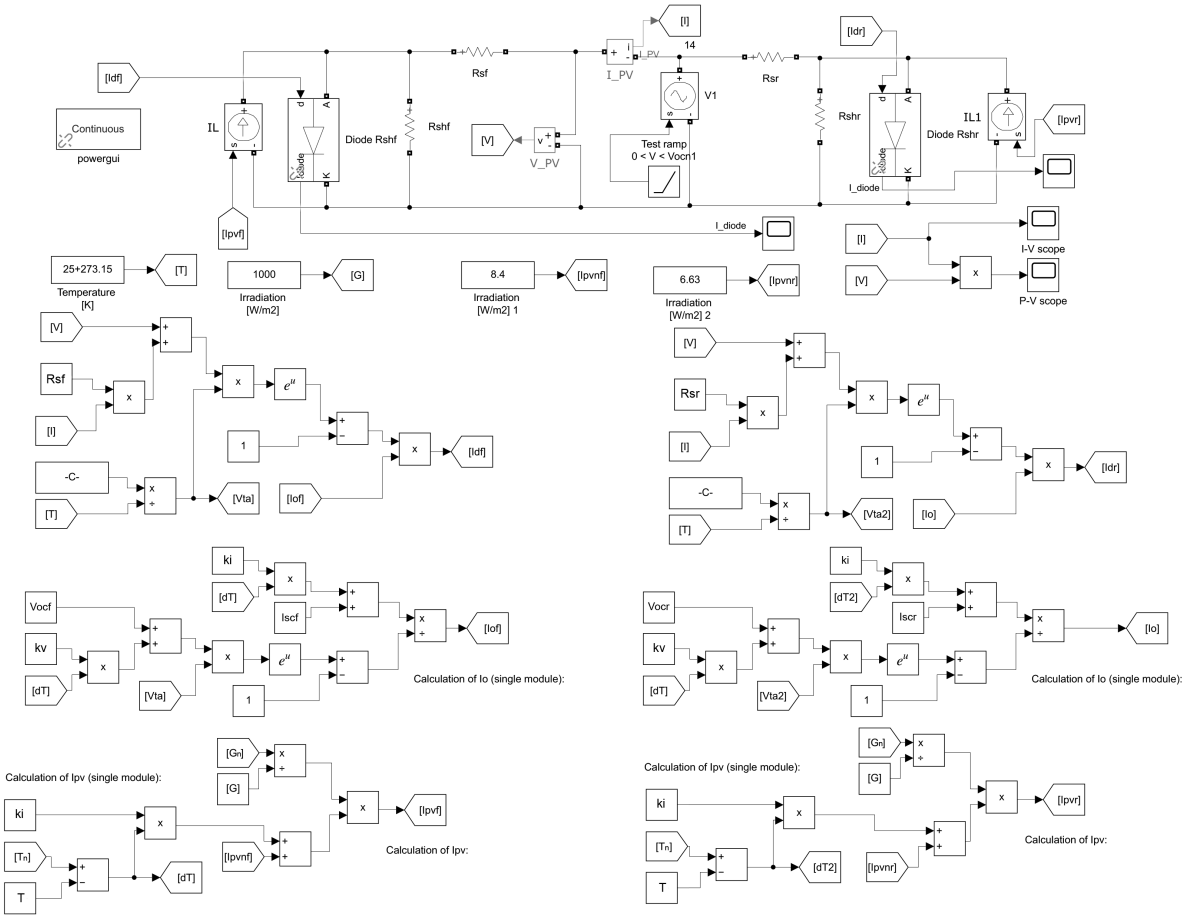

Figure 4.25: Simulink circuit for SDM model

To compare the model predictions with the experimental data, the I-V curve was plotted. The curve illustrated in Fig 4.22, allowed for a comprehensive evaluation of the degree of concurrence between the simulated results and the observed experimental data.

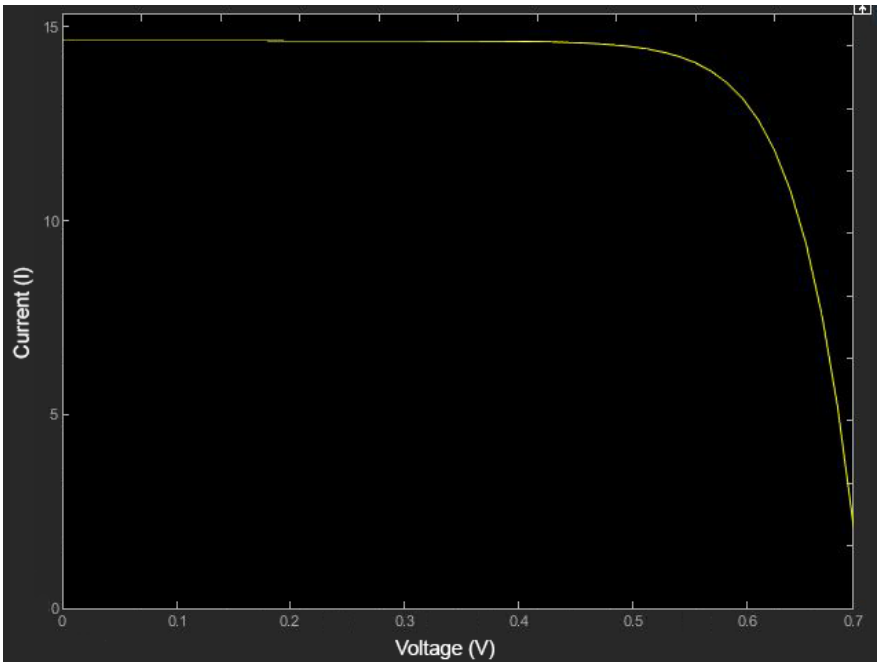

Figure 4.26: Simulation I-V curve

The close alignment between the simulated and experimental IV curves serves as a testament to the fidelity of the chosen model and the accuracy of the extracted parameters. This concurrence strengthens confidence in the predictive capabilities of the model and its ability to accurately represent the performance of the bifacial PV cell in diverse operating conditions (as seen previously with irradiance levels). It also signifies that the selected algorithm or technique successfully captured the essential characteristics of the PV cell and accurately determined the values of the model parameters.

4.5 Conclusion

Our methodology leverages the power of metaheuristic techniques to efficiently explore the parameter space and identify the optimal values that best fit the experimental data. By formulating the parameter extraction as an optimization problem, it was doable to employ diverse algorithms that offer distinct search strategies, to uncover the most accurate parameter values for the single-diode bifacial PV cells. Moreover, the compatibility observed across different irradiation levels underscores the algorithm's versatility and adaptability to real-world operating conditions.Furthermore,after comparing between the used algorithms and PSO and DE,the results were much more compatible using MPA and SOA. Finally to validate the resulting parameters the model was simulated on SIMULINK.

General Conclusion

Solar energy has emerged as the primary energy source for the future, and as a result, the literature on photovoltaics has witnessed rapid growth over the years. In the context of this project, our focus was specifically directed towards the modeling of photovoltaic systems. This particular focus enabled us to acquire a comprehensive understanding of photovoltaics, as embarking on the journey of realizing this project.

Exploring various research domains within the field, ranging from broad areas to more specific ones, proved to be an engaging experience. By considering the bigger picture, a deeper understanding of how the intricate details fit together was grasped, making the work even more captivating.

Our work commenced with a fundamental elucidation of the underlying principle of photovoltaics (PVs), laying a crucial foundation before delving into more intricate aspects. Subsequently, various equivalent models were presented, including the ideal PV cell representation, single-diode model, and double-diode model. In conjunction with these models, the parameters that characterize them were introduced , namely the ideality factor, series resistance, parallel resistance, photo-generated current, and diode saturation current. Building upon this knowledge, light was shed on the novel technology of bifacial cells where the latter structure and working principle , the different types of this technology were described, also a model was proposed for this kind of cells along with the parameters to be obtained.

Obtaining the most accurate five parameters search was the main objective of this project. The single-diode model parameters were identified using two global algorithms (MPA and SOA) that used the I-V experimental data at different levels of irradiation. Global algorithms showed a satisfying estimation as the ten parameters were extracted with slight errors. The results have proved that the Marine Predator Algorithm was better for the search. Finally, it is to be emphasized that the main objective of this work is achieved as the two global algorithms that were employed, extracted bifacial PV single-model parameters with high accuracy.

a further work on parameters identification is required by the use of more sophisticated search algorithms. The features of the algorithms explored in this work can be combined by developing a hybrid algorithm adapted to the parameters search. Also, performing the process with different accuracy metrics as objective functions contributes to a better assessment of tested algorithms. Also better results might be obtained in case of using the double diode model which takes into account the effect of recombination that takes place in the space-charge zone by introducing another diode in parallel.

References

[1] Cayetano López. *Current Challenges in Energy*. BBVA, Madrid, 2008.

[2] Manbir Sodhi, Lennart Banaszek, Chris Magee, and Mercedes Rivero-Hudec. Economic lifetimes of solar panels. March 2022.

[3] J. Appelbaum. Bifacial photovoltaic panels field. *Renewable Energy*, 85:338–343, 2016.

[4] Mark V. Fedkin. Types of PV technology and recent innovations. https://www.education.psu.edu/eme812/node/608. Accessed: 2023-04-29.

[5] National Energy Foundation. Types of Photovoltaic (PV) Cells. Available at: http://www.nef.org.uk/knowledge-hub/solar-energy/types-of-photovoltaicpv-cells.

[6] Stefan Krauter. *Solar Electric Power Generation - Photovoltaic Energy Systems*. Rio de Janeiro: springer, 2006.

[7] How pv cells work. http://www.fsec.ucf.edu/en/consumer/solar$_e lectricity/basics/how_p v_c ells_w ork.html$.

[8] Hadi Afrouzi, Saeed Mashak, Zulkurnain Abdul-Malek, Kamyar Mehranzamir, and Behnam Salimi. Solar array and battery sizing for a photovoltaic building in malaysia. *Jurnal Teknologi*, 64, 10 2013.

[9] PV Education, Available at: urlhttp://www.pveducation.org. [Accessed: May 2023].

[10] Experiment 15 temperature dependence of the saturation current of a junction diode. Solid state physics laboratory, california polytechnic state university.

[11] PV Education. Series resistance, Available at: https://www.pveducation.org/pvcdrom/solar-cell-operation/series-resistance. [Accessed: May 2023].

[12] Ibrahim El Boujdaini. *Impact analysis of the operating temperature of solar inverters*. PhD thesis, 06 2021.

[13] Zhaoning Song, Chongwen Li, Lei Chen, and Yanfa Yan. Perovskite solar cells go bifacial—mutual benefits for efficiency and durability. *Advanced Materials*, 34(4):2106805, 2022.

[14] R. Guerrero-Lemus, R. Vega, Taehyeon Kim, Amy Kimm, and L.E. Shephard. Bifacial solar photovoltaics – a technology review. *Renewable and Sustainable Energy Reviews*, 60:1533–1549, 2016.

[15] Claudia Duran. *Bifacial Solar Cells : High Efficiency Design, Characterization, Modules and Applications*. PhD thesis, Universität Konstanz, Konstanz, 2012.

[16] Wenbo Gu, Tao Ma, Salman Ahmed, Yijie Zhang, and Jinqing Peng. A comprehensive review and outlook of bifacial photovoltaic (bpv) technology. *Energy Conversion and Management*, 223:113283, 2020.

[17] Tobias Fellmeth, Sebastian B. Meier, Elmar Lohmüller, and et al. Industry related approaches for bifacial p-type perx solar cells. *Japanese Journal of Applied Physics*, 57(8S3):08RB18, 2018.

[18] Nico Wöhrle, Elmar Lohmüller, Max Mittag, and et al. Solar cell demand for bifacial and singulated-cell module architectures. 2017.

[19] M. I. U. Haque, Charles Dickens Tusha Falia, and Mahmudul Hasan. Investigating the performance of nanocrystalline silicon hit solar cell by silvaco atlas. *2019 22nd International Conference on Computer and Information Technology (ICCIT)*, 2019.

[20] Chien-Chih Huang, Tinghuan Yang, Ling-Yu Wang, and et al. Tcad modeling of interdigitated back contact solar cells with hybrid diffusion and tunnel oxide passivated contacts. *2021 IEEE 48th Photovoltaic Specialists Conference (PVSC)*, 2021.

[21] Anton Nygren and Elin Sundström. Modelling bifacial photovoltaic systems. *Malardalen university sweeden*, June 2021.

[22] F. I. Barro, M. Sané, and B. Zouma. Theoretical investigation of base doping and illumination level effects on a bifacial silicon solar cell. *Current Journal of Applied Science and Technology*, 7(6):610–618, Mar. 2015.

[23] Byeong Gwan Bhang, Wonbin Lee, Gyu Gwang Kim, Jin Ho Choi, So Young Park, and Hyung-Keun Ahn. Power performance of bifacial c-si pv modules with different shading ratios. *IEEE Journal of Photovoltaics*, 9(5):1413–1420, 2019.

[24] F. I. Barro, M. Sané, and B. Zouma. Theoretical investigation of base doping and illumination level effects on a bifacial silicon solar cell. *Current Journal of Applied Science and Technology*, 7(6):610–618, Mar. 2015.

[25] Mohammed A. A. Al-qaness, Ahmed A. Ewees, Hong Fan, and et al. Marine predators algorithm for forecasting confirmed cases of covid-19 in italy, usa, iran and korea. *International Journal of Environmental Research and Public Health*, 17(10), 2020.

[26] Fatma A. Hashim and Abdelazim G. Hussien. Snake optimizer: A novel meta-heuristic optimization algorithm. *Knowledge-Based Systems*, 242, 2022.

[27] Hamza Belmadani, Aissa Kheldoun, Rafik Bradai, Saad Mekhilef, and Marif Daula Siddique. A twofold hunting trip african vultures algorithm for the optimal extraction of photovoltaic generator model parameters. *Energy Sources, Part A: Recovery, Utilization, and Environmental Effects*, 44(3):7001–7030, 2022.

[28] János Pintér. Global optimization. From MathWorld–A Wolfram Web Resource, created by Eric W. Weisstein, Available at: https://mathworld.wolfram.com/GlobalOptimization.html.

[29] Dalia Yousri, Thanikanti Sudhakar Babu, Eman Beshr, and et al. A robust strategy based on marine predators algorithm for large scale photovoltaic array reconfiguration to mitigate the partial shading effect on the performance of pv system. *IEEE Access*, 8, 2020.

[30] Afshin Faramarzi, Mohammad Heidarinejad, Seyedali Mirjalili, and Amir H. Gandomi. Marine predators algorithm: A nature-inspired metaheuristic. *Expert Systems with Applications*, 2020.

[31] Vun Jack Chin, Zainal Salam, and Kashif Ishaque. An accurate modelling of the two-diode model of pv module using a hybrid solution based on differential evolution. *Energy Conversion and Management*, pages 42–50, 2016.

[32] Mohamed Abdel-Basset, Reda Mohamed, Mohamed Elhoseny, and et al. A hybrid covid-19 detection model using an improved marine predators algorithm and a ranking-based diversity reduction strategy. *IEEE Access*, PP:1–1, 2020.

[33] Wikipedia. Optimization problem, Available at: https://en.wikipedia.org/wiki/Optimization_problem. Accessed on May 8, 2023.